HIGH FREQUENCY EFFECTS OF VARIABLE FREQUENCY DRIVES (VFD) ON ELECTRICAL SUBMERSIBLE PUMP (ESP) SYSTEMS

A Thesis

by

ESRA OZKENTLI

Submitted to the Office of Graduate Studies of
Texas A&M University
in partial fulfillment of the requirements for the degree of

MASTER OF SCIENCE

August 2012

Major Subject: Electrical Engineering

High Frequency Effects of Variable Frequency Drives (VFD) on Electrical Submersible

Pump (ESP) Systems

HIGH FREQUENCY EFFECTS OF VARIABLE FREQUENCY

DRIVES (VFD) ON ELECTRICAL SUBMERSIBLE PUMP (ESP)

SYSTEMS

A Thesis

by

ESRA OZKENTLI

Submitted to the Office of Graduate Studies of
Texas A&M University
in partial fulfillment of the requirements for the degree of

MASTER OF SCIENCE

Approved by:

Chair of Committee,   Hamid Toliyat
Committee Members,   Garng M. Huang
    Aniruddha Datta
    Won-Jong Kim
Head of Department,   Costas N. Georghiades

August 2012

Major Subject: Electrical Engineering

ABSTRACT

High Frequency Effects of Variable Frequency Drives (VFD) on Electrical Submersible

Pump (ESP) Systems. (August 2012)

Esra Ozkentli, B.S., Istanbul Technical University, Istanbul

Chair of Advisory Committee: Dr. Hamid Toliyat

Variable frequency drives (VFD) and subsea (umbilical) cables are frequently used in electrical submersible pump (ESP) systems for offshore platforms. There are two basic system configurations for ESP systems; VFD can be installed on the platform and the motor is connected to it through an umbilical cable, and VFD and the motor are installed closely and they are connected to the system through an umbilical cable.

In this thesis, the pros and cons of each configuration are mentioned, but the focus is on the system with a VFD controlled motor through a long umbilical cable. A 36-pulse VFD is studied. Since multilevel VFDs have high frequency harmonics, high frequency modeling of the umbilical cable is used, and skin effect is also taken into consideration in the cable. The effect of the interactions between the umbilical cable and high frequency harmonics on the motor terminal voltage is explored.

I dedicate this work to

The only God, the merciful, and "His" beloved one,

My grandma & My family

ACKNOWLEDGEMENTS

TABLE OF CONTENTS

LIST OF FIGURES

LIST OF TABLES

1. INTRODUCTION AND LITERATURE REVIEW

As the oil reserves on the mainland have decreased, the oil companies started to extend their oil research area to offshore, thus offshore power systems have become enormously important. However, pumping oil from deep water is facing with different challenges related to the power system components.

Variable Frequency Drives (VFDs) are widely used in offshore-oil pumping systems due to the several advantages they offer to offshore oil pumping systems. Firstly, VFDs are important for motor starting issues. Cross-line starting and reduced voltage starting are traditional ways of motor starting. Neither of these traditional methods offers flexible starting for motors. Especially with cross-line starting, large amount of stress is applied on the motor due to the highest inrush currents as compared to the other methods. However, VFDs offer more flexible starting for motors with a constant volt per hertz method. In this case, voltage and frequency applied to the motor are started from smaller values and increased correspondingly; the ratio between voltage and frequency stays constant. Thus, this soft starting reduces the possibility of drawing sand in and cracks on the shaft. Another advantage of VFDs is being more efficient than throttling control valves in order to adjust the pressure in the oil well. Moreover, the dc bus capacitor allows the system run through during the case of a voltage sagging. However, the systems with VFDs contain some harmonics which cause resonance issues

_____

This thesis follows the style of *IEEE Transactions on Magnetics.*

especially if the system has subsea cables. Depending on system configuration, series or parallel resonances could cause higher harmonic distortions in the system.

Electric submersible pumps (ESP) are efficient to use for oil production and are widely used in offshore oil production systems. Subsea cables are necessary for offshore ESP system installations [1]. Depending on the system requirements, there are different system configurations. Some systems require VFD installations near the motor which are connected through a subsea cable, often called as umbilical cable, to a source. On the other hand, some systems have a long cable installed between the VFD and the motor. Reference [1] indicates that there are several issues related to ESP systems, thus the system should be optimally designed in order to avoid undesired problems such as parallel resonance, series resonance, high harmonic distortion, motor starting difficulty, etc. The harmonics generated by the VFD could coincide with the resonance frequency of the umbilical cable, and cause high voltage spikes on the motor terminals which curtail the isolation of the motor windings. Therefore, the system should be designed properly to reduce the drawbacks of VFDs and umbilical cable.

1.1   Application of MV Drives and Technical Challenges

Most of the installed MV drives have power ratings between 1 and 4MW, and their voltage range is between 3.3kV and 6.6kV even though the power ratings can be up to 40 MW, and voltage ratings can be up to 13.8kV as shown in Figure 1. Most of the load types of the MV drives comprise of fans, pumps, compressors and conveyors.
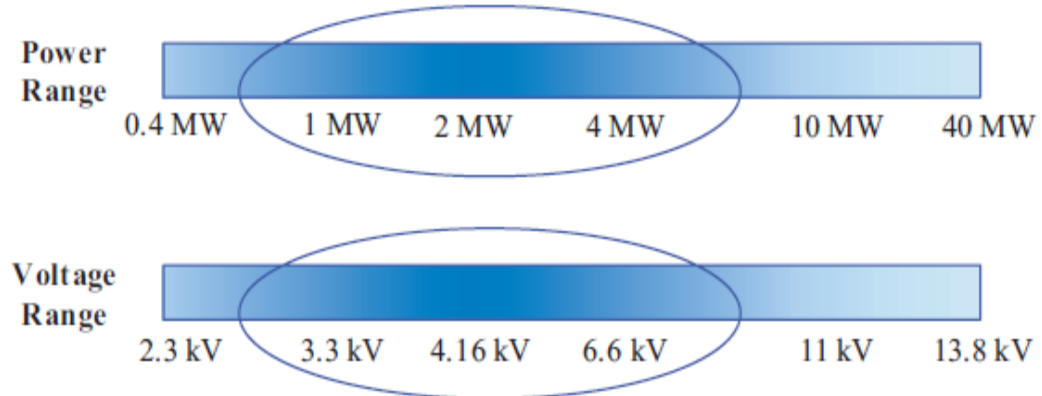
Figure 1: Voltage and Power Ratings of MV Drives [2]

Figure 2 shows the distribution of the load types for MV drives, and shows the market search which tells only 3% of the installed MV drives is variable speed drives. It is stated that with MV drives, it is possible to save significantly on energy cost and the payback time of a MV variable speed drive is between one and two and a half years [2].
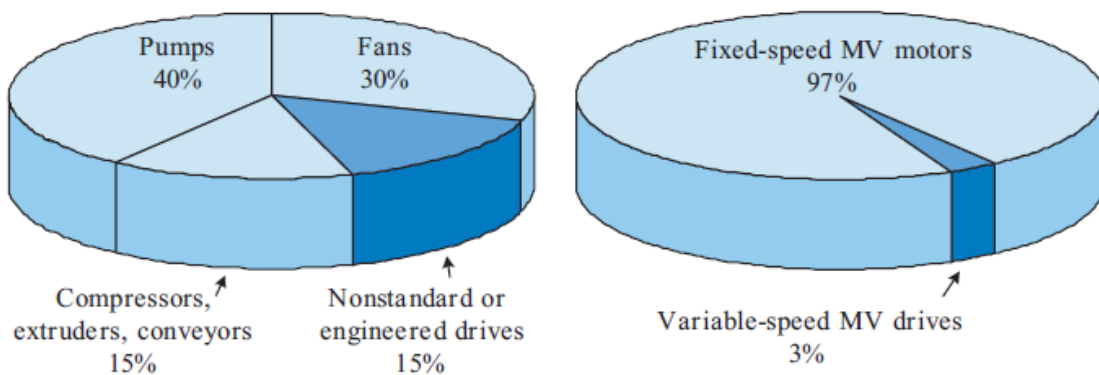
Figure 2: Load Types of MV Drives and Percentage of MV Drives [2]

A general block diagram of a MV drive is shown in Figure 3. Line-side and motor-side filters can be used if they are necessary depending on the system conditions. Multiple winding, phase shifting transformer is generally used to reduce the line-side current distortions. Diodes or SCRs are commonly used for multi-pulse rectifiers. A capacitor is used in order to have less ripple voltage waveform on the dc-bus for voltage source drives (VSI), and an inductance is used to smooth the current for current source drives (CSI). An adjustable magnitude and frequency voltage can be obtained by VSIs and adjustable three-phase current can be produced by CSIs.
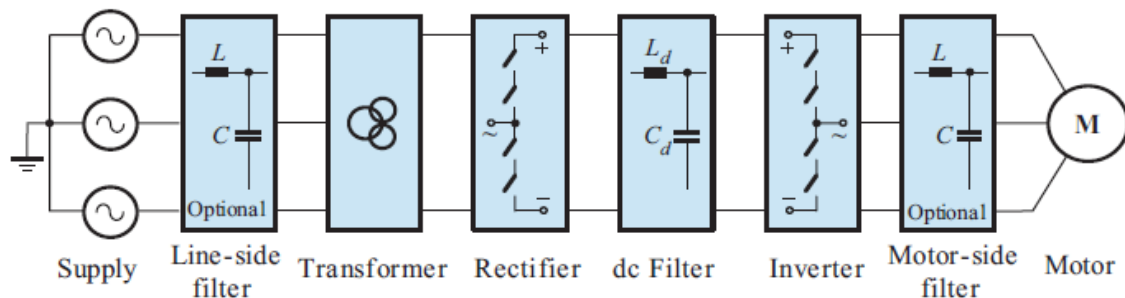
Figure 3: Block Diagram of MV Drives [2]

The systems with MV drives are facing with different challenges which can be categorized into three groups; line-side power quality requirements, motor-side converter design, and switching device operating limits [2].

1. Line-Side Challenges:

According to IEEE Standard 519-1992, there are upper limits for voltage and current harmonic distortions depending on the system. The rectifier in the motor drive draws certain amount of harmonic currents which causes some notches in voltage waveforms and causes some problems on the system such as transformer overheating,

failure of some equipments, data loss on computers, false tripping of protective devices, etc. Therefore, the rectifier should adhere to the regulations explained in the standard. Phase shifting transformers are commonly used with multi-pulse rectifiers in order to meet the requirements.

Most of the time, satisfying the high input power factor, which is 0.9 or above, is a general requirement for the electric devices. Motor drives should meet the criteria depending on the system they are used in. In order to improve power factor or reduce current distortion, line side capacitors can be installed in the system with the risk of LC resonance issues. The capacitor may create a resonant circuit interacting with the line inductance, which results in high oscillations or over voltages when the harmonic currents by rectifier coincide with that LC resonance frequency. The switching devices may be destroyed if the LC resonance issue is not considered in the design stage.

2. Motor-side Challenges:

Depending on the dc-bus voltage magnitude and the switching speed of the devices in MV drives, dv/dt value is determined, and high values of dv/dt could cause severe problems on motors. Induced voltage between rotor and stator due to high dv/dt causes current flowing into the shaft bearing, resulting early bearing failure. High dv/dt could also cause voltage doubling effect. When there is a long cable (longer than critical cable lengths), due to the mismatch of the impedances between the cable and the motor, voltage waves are reflected back which can double the voltage on motor terminals. Critical cable lengths are defined in [2] as about 100m for 500V/μs, 50m for 1000V/μs, and 5m for 10,000V/μs. Multi-level inverters are used to decrease dv/dt level in order to

reduce the drawbacks of the fast switching. Figure 4 and Figure 5 show phase-to-phase voltage waveforms of a two-level inverter output and a seven-level H-bridge inverter respectively. If the same output magnitude wants to be obtained, it is clear from the figures that 7-level H-bridge inverter has lower dv/dt due to smaller voltage steps.
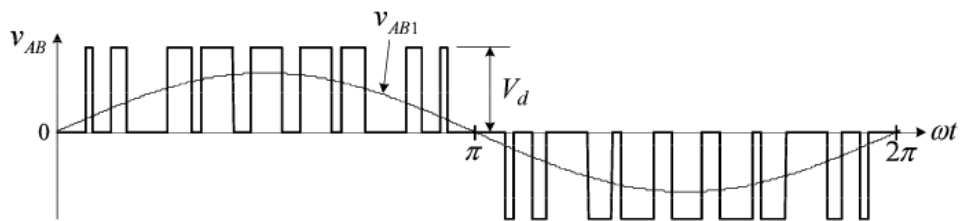
Figure 4: Two-level Inverter Output Waveform [2]
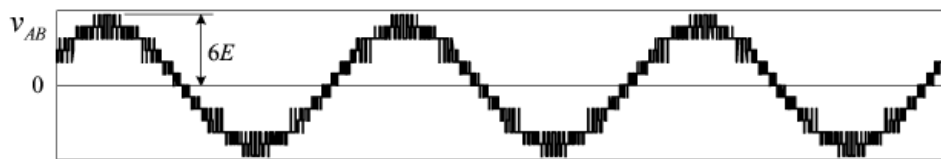
Figure 5: 7-level H-bridge Inverter [2]

Another problem about switching is common-mode voltage explained in [2] that it generally occurs due to the switching of inverters. This voltage is seen on the neutral point of the stator winding with respect to the ground, causing premature failure of the winding insulation.

Harmonics also cause problems on the motor side. Since the motor torque is proportional to the motor current, harmonics in the current causes some torque pulsations which may lead torsional vibration when the frequency of torque pulsations coincide with the natural frequency of the mechanical system. Another effect of

harmonics is related to power losses on the motor. Additional power losses on the winding and on the magnetic core occur because of the harmonics in the voltage and the current waveforms. This is called motor derating which causes motor not to be able to operate at its full capacity.

Resonance is another problem on the motor-side which may happen in the presence of harmonics when harmonic voltages excite the resonant circuit. Resonant circuit may occur because of the interaction between the motor-side filter capacitor and the motor inductance or long cable between the motor drive and the motor. Although cable resistances or motor winding resistances provide some damping, this issue should be considered carefully at the early stage of the design of the drive system.

3. Switching device challenges:

The switching frequency of the switching devices should be limited because lower switching leads lower power losses. Cooling requirements for switching devices is another reason for upper limits of switching. However, lower switching frequencies causes more harmonic distortions on the output waveforms of the drive.

Another problem related to switching devices is that since they all have different static and dynamic characteristics, the voltage is not shared equally among them in the blocking mode when they are connected in series.

1.2 Applications of Subsea Cables and Technical Challenges

Subsea cables are very common in the electrical submersible pump (ESP) systems for offshore platforms. Challenges of VFDs in the system combined with long

cables may cause serious issues depending on the system configuration. Figure 6 and Figure 7 show two typical configurations for subsea ESP systems.
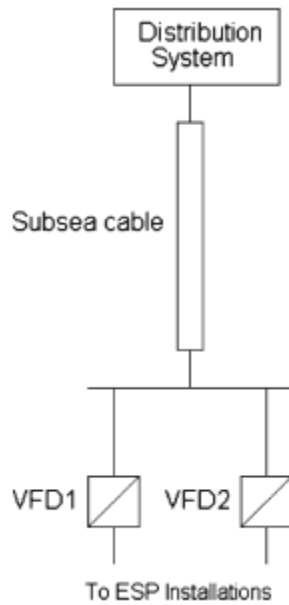
Figure 6: Configuration 1 [1]
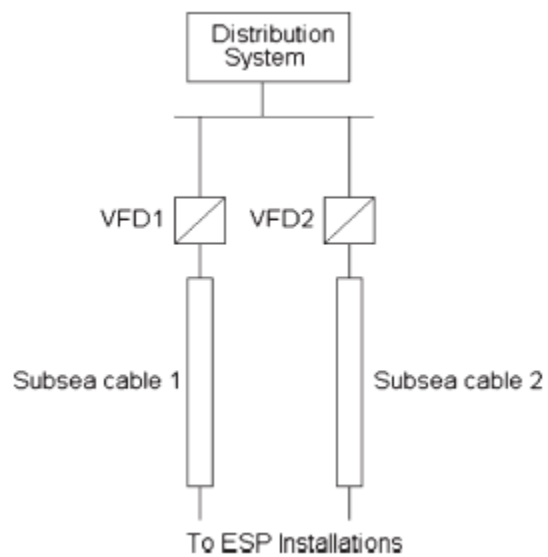
Figure 7: Configuration 2 [1]

ESP systems similar to configuration 1, shown in Figure 6, have an advantage of supporting numerous VFD-ESP wells. Another advantage of configuration 1 over configuration 2 is that the cables between VFDs and ESP motors are considerably shorter downhole cables enabling easier motor starting. However, the main problem with configuration 1 is the parallel resonance issues. Length of the subsea cable, cable parameters, and VFD type are the factors which affect the parallel resonance. Certain types of VFDs draw certain dominant harmonic currents; for example 5th harmonic dominates for 6-pulse VFDs, 12-pulse VFD draws 11th harmonic mostly, and etc. When those harmonics coincide with the resonance frequencies of the cables (resonance frequency of cables depend on the cable parameters), the magnitude of those harmonics are amplified, and total harmonic distortion of the line current on the distribution-side of the cable becomes worse than VFD-side of the cable. Figure 8 and Figure 9 are taken from the reference [1] which shows the difference between the current waveforms at the distribution-side and the VFD-side of the cable (the currents are given as the percentage of the fundamental current). Since the system has 6-pulse VFDs, the 5th harmonic is dominant in the waveforms and it is about 9.6% on the load side and about 88.3% on the distribution side of the subsea cable. The cable creates a resonant circuit for the 5th harmonic, thus the 5th harmonic magnitude is amplified and caused a bigger distortion on the distribution side of the cable as it is shown in Figure 9. As it is clear in this example, if the system is not analyzed carefully, severe effects of parallel resonance may occur in the system.
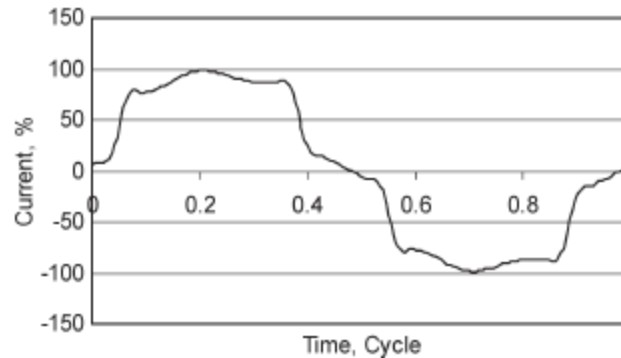
Figure 8: Current Waveform at the VFD-side of the Cable for Configuration 1 [1]
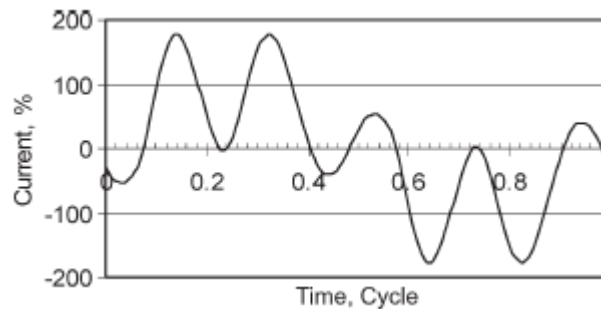
Figure 9: Current Waveform at the Distribution-side of the Cable for Configuration 1 [1]

ESP systems similar to configuration 2, shown in Figure 7, could only support a single ESP well with a subsea cable. The subsea cable could be so long between the VFD and the ESP motor that severe voltage drops may occur, causing difficulty in starting the motor. Another problem with this configuration is that, series resonance occurs in the system. However, C filter, RC filter, RLC filter, or LC filter is good enough to attenuate the resonance points in this configuration. In reference [1], a simple example is given for series resonance problem. Figure 10 shows the frequency response of a 2.5km subsea cable and 1.5km downhole cable, and the motor. It is clear that there is a resonance point at 3779 Hz on the cable circuit and the VFD produces harmonics

around this frequency. Thus, due to the voltage amplification, voltage spikes occur in the system. Figure 11 and Figure 12 show the waveforms of the motor and the cable before and after a filter installed in the system respectively.
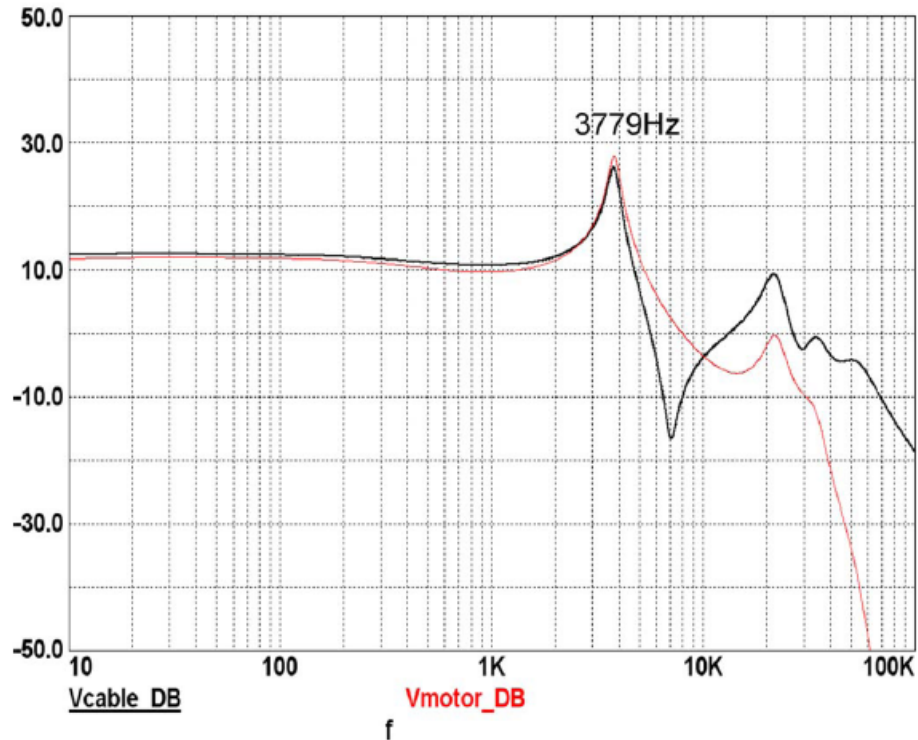
Figure 10: Frequency Response the Subsea Cable and the Motor [1]
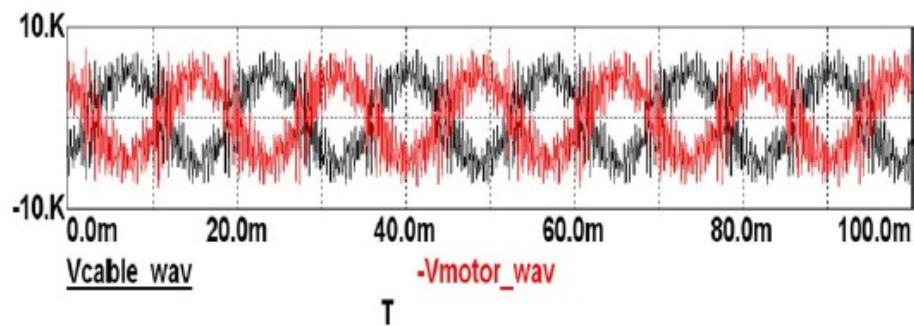
Figure 11: Voltage Waveforms of the Cable and the Motor [1]
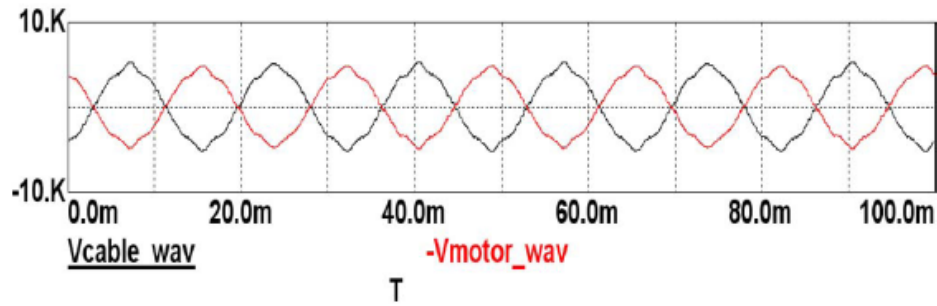
Figure 12: Voltage Waveforms of the Cable and the Motor after a Filter Installed [1]

Another issue for configuration 2 is motor starting since the subsea cable could be very long. During motor starting, the current is around 2 times rated current with a VFD. With VFD, lower voltage and lower frequency is applied to the motor during starting; motor may not get started easily since the voltage drop is high due to the higher current and the resistance of the long cable. Shortly, for long cable lengths, this issue might become a more severe problem than shorter distances. Therefore, voltage drop studies and motor starting studies should be performed during the early design stage of the system.

1.3   Research objectives

The objective of this thesis is to show the high frequency effects of variable frequency drives (VFD) and long umbilical cables in electrical submersible pump (ESP) systems for offshore platforms. Umbilical cables will be modeled for high frequencies including their skin effects, and the frequency analysis of the cable will be performed in order to understand the system behavior. 36 pulses, multi-level VFD will be modeled,

and interactions with the umbilical cable will be studied. Resonance issues will be addressed in the system, and the effect of resonances on the motor terminal voltages plus effect of the skin effect on the cable will be discussed. Finally, the effects of a passive filter in the system will be studied and the simulation results will be given.

1.4   Thesis outline

This thesis is organized into five chapters. The first chapter presents an overview of the problems associated with ESP systems for offshore platforms. The second chapter explains the accurate modeling of umbilical cables including their skin effect, and performs the frequency analysis of the cables. In the third chapter, medium voltage variable frequency drive (VFD) components and different VFD topologies are explained along with the comparison of the different topologies. In the fourth chapter, different components of an example system are introduced, and the simulation results and discussions are given. In the final chapter, conclusions and recommendations for future work is included.

2. MODELING OF UMBILICAL CABLES

2.1 Π-model of Cables

According to IEEE Standard 519-1992, a cable or a line longer than 250 km is considered a long cable or a long line for a 60-Hz system and can be modeled as shown in Figure 13.
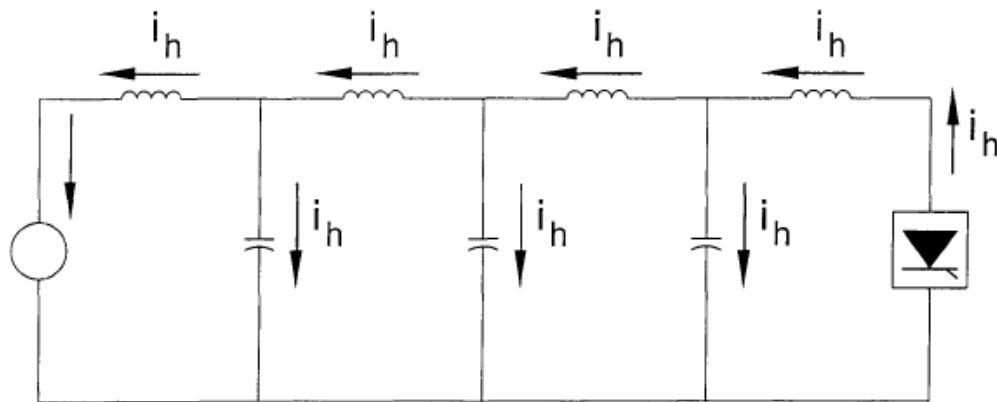
Figure 13: Long Line Equivalent Circuit

Transmission lines up to 80km are considered as short lines which can be modeled without the shunt capacitors. Even though the subsea cables are generally up to 60-80km long, the model for subsea cables should include the shunt capacitors. The reason is that, the shunt capacitors can be too large to ignore for higher frequencies, whereas it can be ignored for fundamental frequency. Since subsea systems include high

harmonics frequently (due to the usage of multi-level VFDs), the shunt capacitors should

be included in modeling of the subsea cable even though the lengths are only up to 60km

long. Figure 14 shows a simple lumped Π-equivalent circuit, which can be used to

model subsea cables for offshore power distribution systems [3].
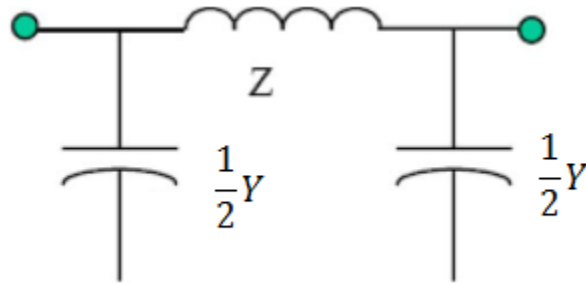
Figure 14: Lumped Equivalent Circuit

Here;

$$z = r + j\omega l$$
$$y = g + j\omega c$$

(2.1)

where z is the series impedance per unit length and y is shunt admittance per unit length.

Multiplying the unit length parameters with the total length of the cable, the total

impedance and the total shunt admittance of the cable is calculated. Cascading several π-

sections, one could model cables for certain purposes.

2.2   Determination of Number of π-sections

Although the parameters of the transmission systems are distributed in nature, lumped equivalent circuits are usually used to represent the system. It is important to specify the number of the sections accurately, in relation to a particular study, if lumped parameters are used to model the system [4]. Simple criteria can easily be applied to any study in order to determine the number of π-sections as explained in [4].

Assuming conductance is zero (g = 0), the parameters of the cable can be defined as;

$$Z = R + jX$$
$$Y = jB$$
$$(2.2)$$

Here R is total resistance, X is total inductive reactance and B is total susceptance of the cable which could be calculated as follows if L is the length of the cable.

$$R = r * L$$
$$X = \omega * l * L$$
$$B = \omega * c * L$$
$$(2.3)$$

Then, the number of π-sections N can be calculated as;

$$2N^2 \rangle\rangle |jB * (R + jX)| \qquad (2.4)$$

Figure 15 shows the number of sections calculated for a range of frequency. Curve A represents the number of sections when $2N^2$ is set equal to the right-hand side of the (2.4). Curve B takes into account the multiplying factor which is applicable to wide range of power transmission lines as it is explained in [4].
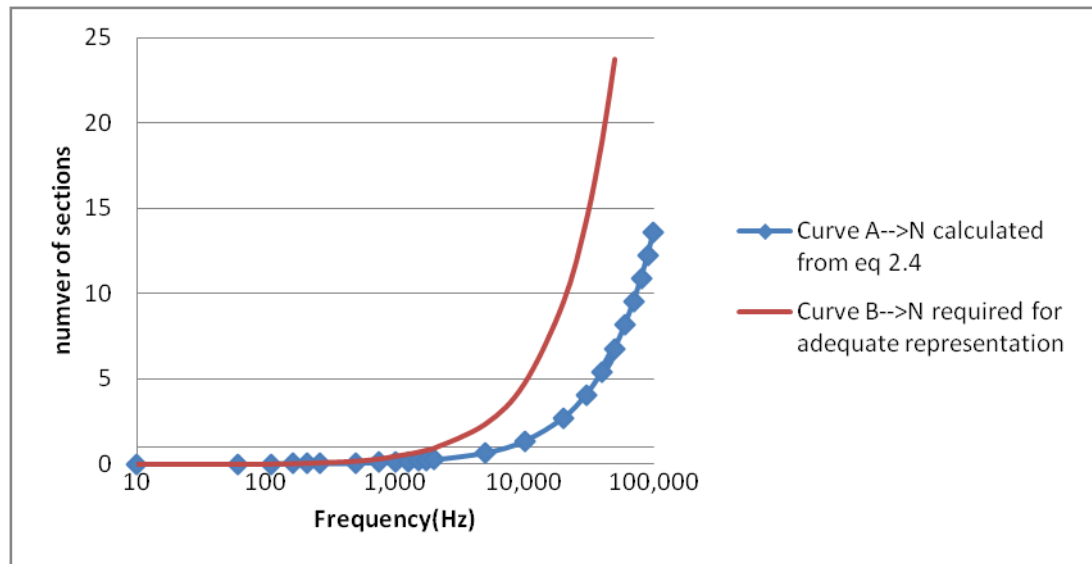
Figure 15: Number of Sections

Depending on the range of frequency which the analysis takes into account, the number of sections could be defined by applying the basic criteria mentioned above. It is important to determine the number of sections in order to represent the transmission line adequately in the frequency range under study. Figure 16-a represents the distributed parameter of a sample cable, Figure 16-b represents one section model of the cable and Figure 16-c represents 5-section model of the cable. It is clear from Figure 16 that, depending on the number of section the cable modeled as, the adequacy of the study would be changed. While one section representation is good for studies up to 1 kHz, the cable representation should be extended to 5 sections when a range up to 10 kHz is considered.
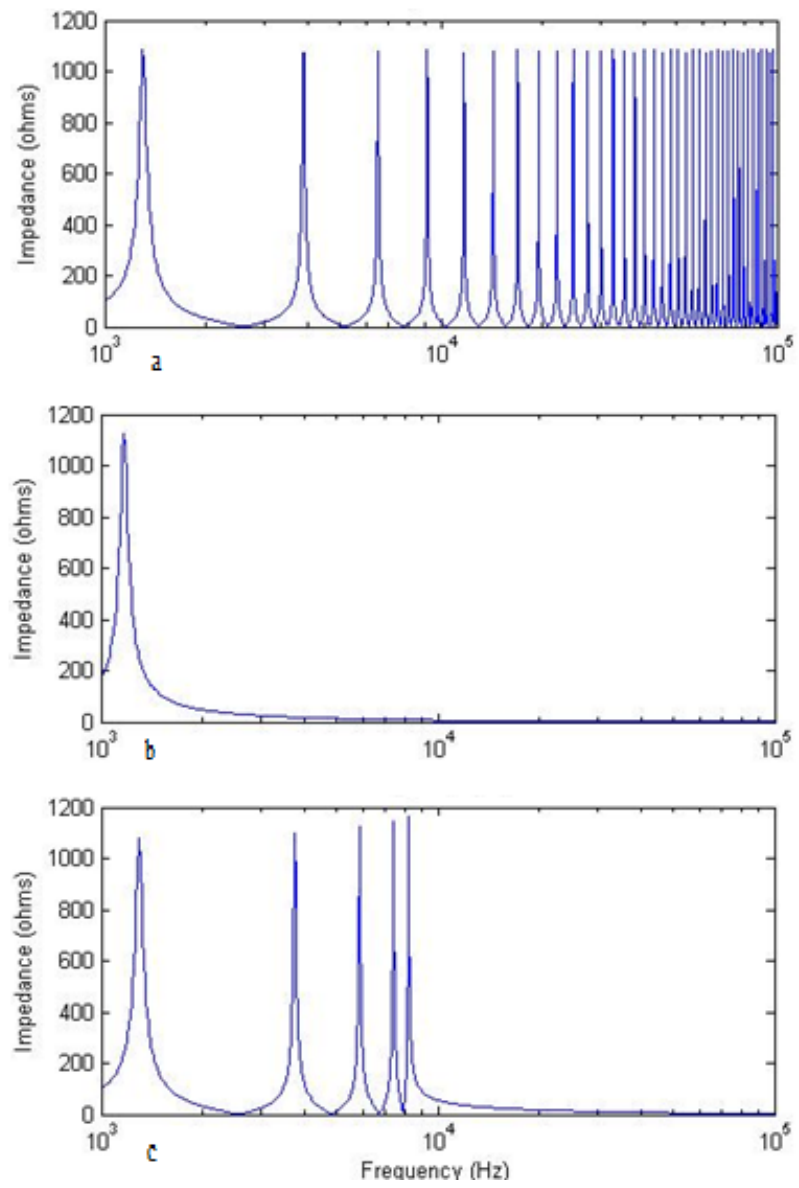
Figure 16: Impedance against Frequency

2.3   Inductance of Coaxial Cables

An inductance is a circuit element that generates an opposing voltage proportional to the change in its current. Inductance calculation for coaxial cables includes two parts [5];

1. Internal Inductance Calculation:

Internal inductance for a straight wire which carries a uniformly distributed dc current equals to;

$$L_{internal} = \frac{\mu_0}{8\Pi} = 50nH/m \qquad (2.5)$$

When ac current flows through a wire, current is not uniformly distributed due to skin effect which is explained in the next section. For high frequencies, current flows through a smaller area on the cross section of the cable (skin depth). Thus, internal inductance decreases as the frequency increases. For wide range frequency analysis required studies, skin effect modeling for cables becomes important.

2. External Inductance Calculation:

Figure 17 shows the cross-section of a coaxial cable, including its shield. Current goes through the wire and returns on the shield. In this case, the external inductance can be calculated as;

$$L_{external} = \frac{\mu_0}{2\Pi} \ln \frac{r_s}{r_w} [H/m] \qquad (2.6)$$
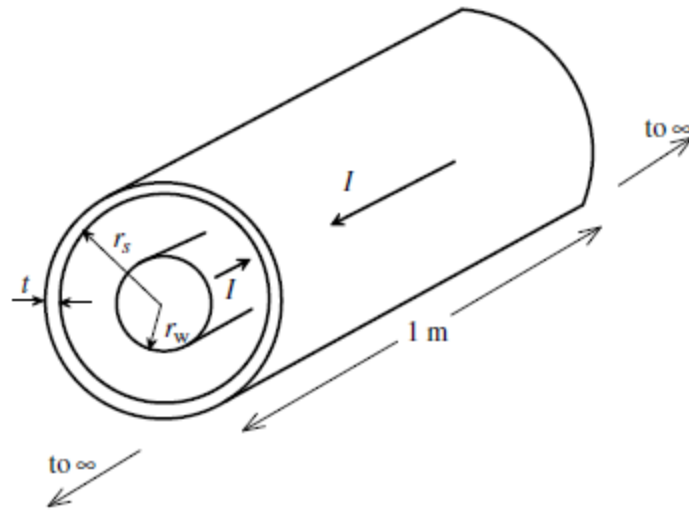
Figure 17: Cross-section of a Coaxial Cable

A three-phase system consists of three separate cables and they are usually installed as either trefoil formation or flat formation which is shown in Figure 18. In such a system, when the shields are grounded, external inductance can be defined as mutual inductance with the other cores.

Mutual inductance per core can be calculated as;

$$L_{mutual} = \frac{\mu_0}{2\Pi} \ln \frac{(K \times S)}{r_w} [mH/km] \tag{2.7}$$

where,
        K=1, for trefoil formation
        K=1.26, for flat formation
        S=distance between conductor of cable axes
        r_w=conductor(wire) radius

Thus, the total impedance per one core of a three-phase system can be calculated as;

$$L = L_{internal} + L_{mutual} \tag{2.8}$$
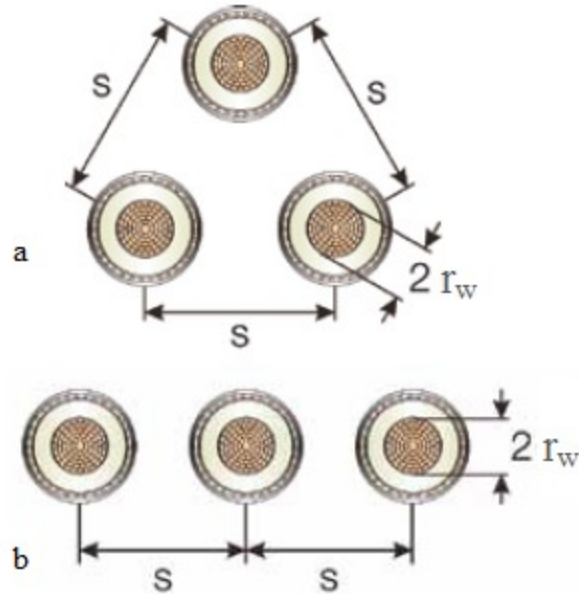
Figure 18: a-Trefoil Formation, b-Flat Formation

2.4 Skin Effect Modeling

When an alternating current flows through a wire, it does not penetrate the entire cross section of a conductor; it tends to flow at the skin (outer layer) of the conductor. In other words, current flows between surface and skin depth of the conductor which decreases as the frequency increases. Thus, resistance of the conductor increases, and internal inductance due to the flux linkage inside of the conductor decreases.

For the systems with 25 km or longer cable lengths, if the system has variable frequency drives which have high harmonic contents in the current and the voltage output waveforms, the skin effect on the impedance and the resistance of cables should be taken into account [6].

Due to the complexity of the frequency dependent parameters, a ladder methodology was proposed to model the skin effect [7]. According to this methodology, conductors can be considered as concentric layers which all have their own resistive and inductive elements. Each branch represents a decade of frequency, and each branch is expected to carry the currents in the range of frequency it is modeled for. This can be modeled as parallel branches consisting of resistive and inductive elements in series which is shown in Figure 19.
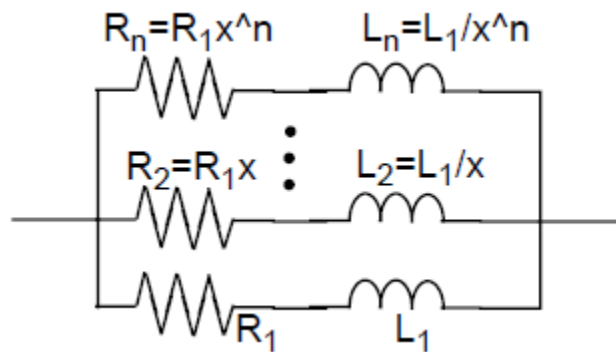
Figure 19: Ladder Circuit for Skin Effect [7]

The ratio between resistors (R_1, R_2, R_3,..) should be constant in order to capture the low pass characteristics of the line [8]. Resistance should be increased by a factor (shown as "x" in Figure 19) and in case of choosing $x=\sqrt{10}$, it is found that one should add one branch to the model for each decade of frequency in order to have a valid model for that frequency range. Similarly, since the inductance is decreasing as the frequency increases, inductor ratio from ring to ring should be decreased by the same factor "x" in order to validate the model for the same frequency range [7]. By this

method, each additional ring will have bigger resistance and smaller inductance representing the nature of any conductor. Table 1 shows the values of R_1 and L_1 depending on the number of rings (branches) used for a model.

Table 1: R and L Factors for Skin Effect

Number of Branches	R_1	L_1
1	R_{DC}	$L_{internal}$
2	1.32 R_{DC}	1.68 $L_{internal}$
3	1.42 R_{DC}	1.94 $L_{internal}$
4	1.45 R_{DC}	2.03 $L_{internal}$
5	1.457 R_{DC}	2.06 $L_{internal}$
6	1.461 R_{DC}	2.07 $L_{internal}$

2.5   Frequency Domain Analysis of Cables

Adjustable speed drives cause harmonics in a system. When these harmonics are close to a resonance frequency, the magnitude of these harmonics might be amplified which results in higher THD (total harmonic distortion) in the system. Then, limiting the amplitude of these harmonics might be required.

Frequency domain analysis of a cable is important in order to perform studies for verifying the performance of systems which consist of variable frequency drives with long cables. In order to determine the resonances in a frequency range, frequency

dependent cable parameters should be used. Frequency dependent cable parameters can be calculated by using finite element method, or by using frequency modeling of the cable as it is mentioned in the previous section.

A coaxial cable with shield is selected to perform the frequency analysis for the two examples below. Data sheet of the cable selected is given in Appendix A**.**
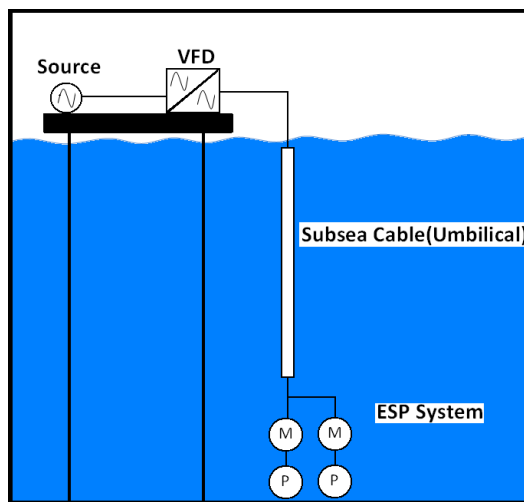
Figure 20: An Offshore System

2.5.1. Example 1

An offshore oil pumping system with a long cable between the drive and the motor is shown in Figure 20. Π-modeling of the cable including its skin effect can be done as it is explained earlier. A 5 km length is picked as the first example. The cable is modeled as 10 π-sections and 3 branches for the skin effect which is a valid model for 3 decades of frequency.

First, total resistive, inductive and capacitive elements per π-section should be calculated as follows.

$$R_{DC-\Pi} = \frac{r \times L}{10} = \frac{0.124(\Omega/km) \times 5(km)}{10} = 0.062\Omega/\Pi-\sec tion \tag{2.9}$$

$$L_{\Pi} = \frac{(l_{int} + l_{mut})L}{10} = \frac{(50+316)(\mu H/km) \times 5(km)}{10} = (25\mu H + 158\mu H)/\Pi-\sec tion \tag{2.10}$$

$$C_{\Pi} = \frac{c \times L}{10} = \frac{0.252(\mu F/km) \times 5(km)}{10} = 0.126\mu F/\Pi-\sec tion \tag{2.11}$$

Second, the parameters (L_1, L_2, L_3, and R_1, R_2, R_3) of the ladder circuit for the skin effect should be calculated. Using Table 1 and choosing the factor x=$\sqrt{10}$, the parameters are calculated as follows;

$$\begin{aligned}
R_1 &= 1.42 \times R_{DC} = 1.42 \times 0.062 = 0.08804\Omega \\
R_2 &= R_1 \times x = 0.08804 \times \sqrt{10} = 0.278407\Omega \\
R_3 &= R_1 \times x^2 = 0.08804 \times 10 = 0.8804\Omega \\
L_1 &= 1.94 \times L_{int} = 1.94 \times 25\mu H = 48.5\mu H \\
L_2 &= L_1/x = 48.5/\sqrt{10} = 15.337\mu H \\
L_3 &= L_1/x^2 = 48.5/10 = 4.85\mu H
\end{aligned} \tag{2.12}$$

Figure 21 shows the ladder model of the Π-sections. The parameters calculated above should be used for each Π-section since the cable is considered 10 identical Π-sections. The capacitor values are identical as well and can be calculated as;

$$C_1 = C_2 = \frac{C_{\Pi}}{2} = 0.063\mu F \tag{2.13}$$
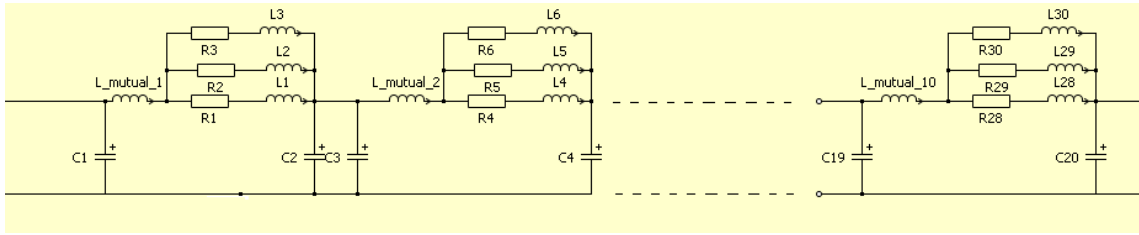
Figure 21: Ladder Model of Π-sections

Figure 22 shows the frequency response of the cable modeled as in Figure 21. The graph shows the ratio of output voltage of the cable to input voltage of the cable in dB which can be calculated as;

$$freq.response[dB] = 20 \times \log_{10}\left(\frac{V_{out}}{V_{in}}\right)$$

(2.14)

It is clear that the first resonance point is about 5kHz point with a magnitude of over 25. First resonant point is important because it is the closest point to the switching frequency of VFDs. If the harmonics caused by VFDs are close to resonant points, their amplitudes are amplified by the ratio of V_{out} /V_{in} of the cable. This results in higher harmonic amplitudes at the output side of the cable where motors are connected. This case is very hazardous for motors and especially for their winding insulations. Since amplitude of the fundamental frequency is not affected by resonance issues, the total harmonic distortion will be higher at the output of the cable. This will cause distortion on the current waveform, leading further problems such as torque pulsations.
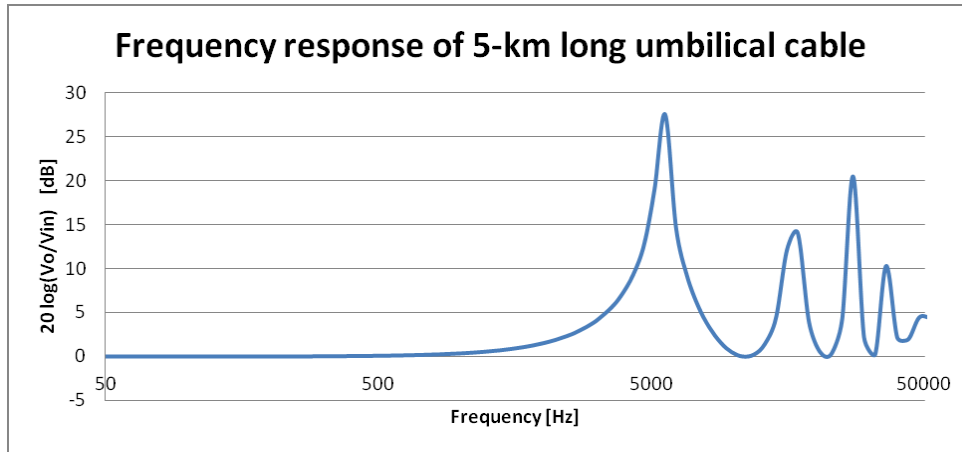
Figure 22: Frequency Response of 5km-long Umbilical Cable

2.5.2. Example 2

An offshore oil pumping system with a long cable between the drive and the motor was shown in Figure 20. A 20 km length is picked in this example, and the calculation way is same as the previous example. The cable is modeled as 45 π-sections and 3 branches for the skin effect which is a valid model for 3 decades of frequency.

First, total resistive, inductive and capacitive elements per π-section should be calculated as follows.

$$R_{DC-\Pi} = \frac{r \times L}{45} = \frac{0.124(\Omega/km) \times 20(km)}{45} = 0.0551\Omega/\Pi \qquad (2.15)$$

$$L_{\Pi} = \frac{(l_{int} + l_{mut})L}{45} = \frac{(50 + 316)(\mu H/km)20(km)}{45} = (22.22\mu H + 140.44\mu H)/\Pi \qquad (2.16)$$

$$C_{\Pi} = \frac{c \times L}{45} = \frac{0.252(\mu F/km) \times 20(km)}{45} = 0.112\mu F/\Pi \qquad (2.17)$$

Secondly, the parameters (L_1, L_2, L_3, and R_1, R_2, R_3) of the ladder circuit for the skin effect should be calculated. Using Table 1 and choosing the factor $x=\sqrt{10}$, the parameters are calculated as follows;

$$
\begin{aligned}
R_1 &= 1.42 \times R_{DC} = 1.42 \times 0.0551 = 0.0782577\Omega \\
R_2 &= R_1 \times x = 0.0782577 \times \sqrt{10} = 0.2474728\Omega \\
R_3 &= R_1 \times x^2 = 0.0782577 \times 10 = 0.782577\Omega \\
L_1 &= 1.94 \times L_{int} = 1.94 \times 22.22\mu H = 43.1068\mu H \\
L_2 &= L_1/x = 43.1068/\sqrt{10} = 13.632\mu H \\
L_3 &= L_1/x^2 = 43.1068/10 = 4.31068\mu H
\end{aligned}
\tag{2.18}
$$

The parameters calculated above should be used for each Π-section shown in Figure 21 since the cable is considered 45 identical Π-sections. The capacitor values are identical as well and can be calculated as;

$$
C_1 = C_2 = \frac{C_\Pi}{2} = 0.056\mu F
\tag{2.19}
$$

Figure 23 shows the frequency response of the 20-km long cable modeled as in Figure 21. The graph shows the ratio of output voltage of the cable to input voltage of the cable in dB which can be calculated as;

$$
freq.response[dB] = 20 \times \log_{10}\left(\frac{V_{out}}{V_{in}}\right)
\tag{2.20}
$$
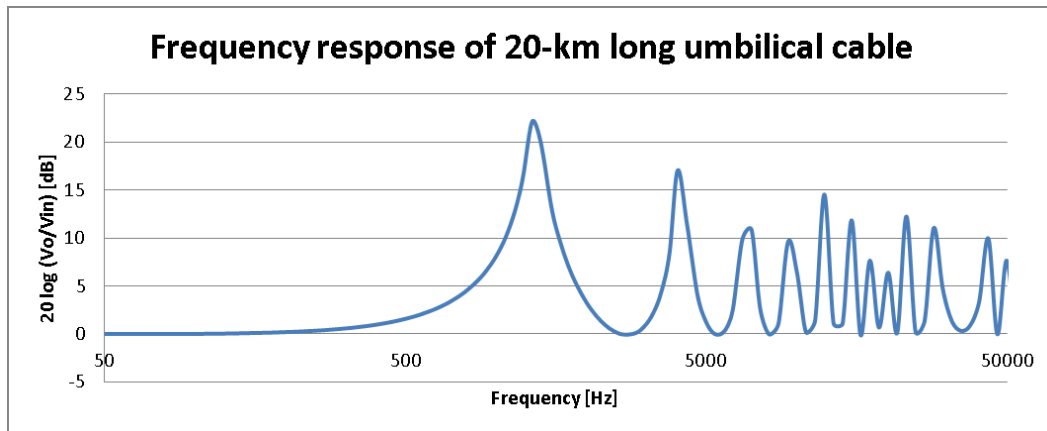
Figure 23: Frequency Response of 20-km Long Umbilical Cable

In this example, the first resonance happens around 1.3 kHz with a magnitude of over 20. This might be critical if the switching frequency of the VFD in a system is 600 Hz. The harmonics will be higher in magnitude around the double of the switching frequency, resulting in significant harmonic amplitudes on the output side of the cable where the motor is connected. Therefore, frequency analysis of the system should be done, and the critical frequency ranges should be determined in order not to have any hazardous effects on insulations and on the entire system.

2.6   Comparison of Frequency Dependent and 50-Hz Parameters of Cables

It is also possible to model cables with their 50 Hz parameters. That model assumes that, the current flows almost through the entire cross-section of the cables, and the cables have the same resistance and inductance values for all frequencies. However, this is not an accurate way of modeling cables since values of the parameters are subject

to change in practice as frequency changes. Figure 24 shows the difference between 50 Hz values of the 20-km long cable and its frequency dependent values.
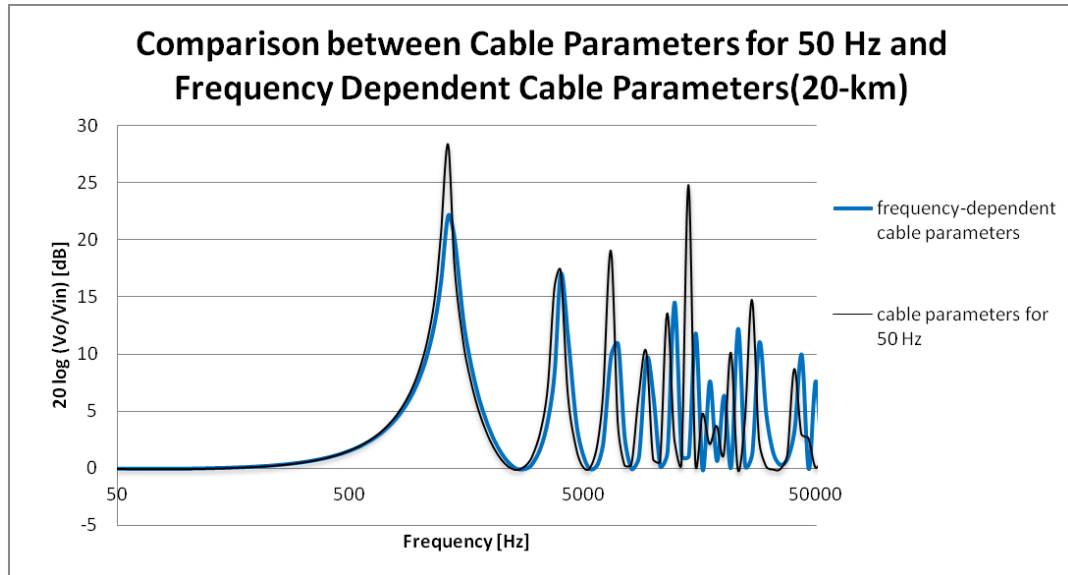
Figure 24: Comparison between 50 Hz Values and Frequency Dependent Values of the 20-km Long Umbilical Cable

Figure 25 shows the difference between 50 Hz values of the 5-km long cable and its frequency dependent parameters. It is clear that frequency dependent parameters give less pessimistic results. It can be observed that, since the resistance value increases as frequency increases, the ratio V_o/V_{in} is smaller than constant parameters. Moreover, resonant points are slightly shifted away due to the decrease in inductance values and no change in capacitance values of the cable. These results show that the method applied for skin effect modeling is valid for coaxial cables.
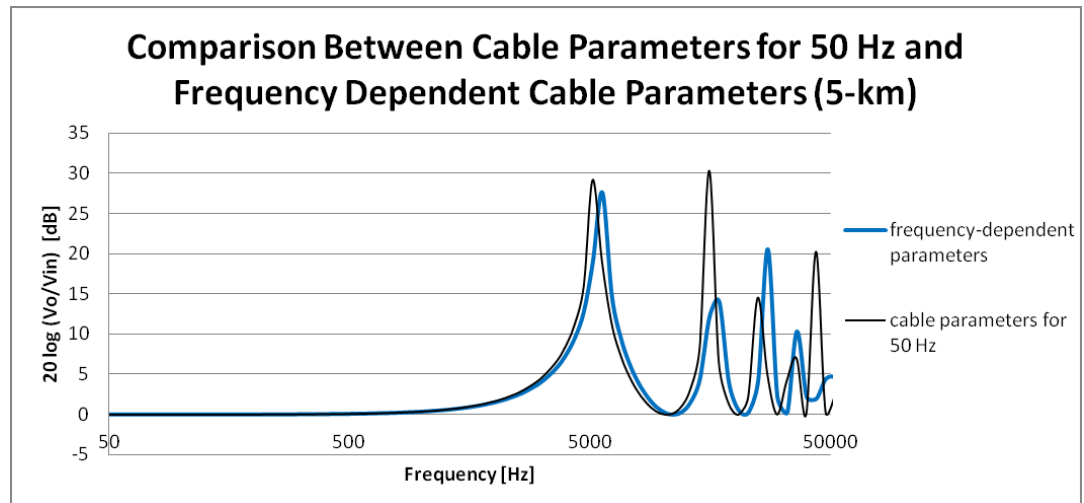
Figure 25: Comparison between 50 Hz Values and Frequency Dependent Values of the 5-km Long Umbilical Cable

3. MEDIUM VOLTAGE VARIABLE FREQUENCY DRIVES

Variable Frequency Drives (VFD) are connected between a utility power system (or voltage source e.g. a generator) and induction motors, and they are used for controlling induction motors. VFDs must be able to adjust the output frequency and voltage, and maintain continuous rated current at any frequency. Medium voltage drive power ratings change from 0.4 MW to 40 MW, and voltage ratings vary between 2.3 kV to 13.8kV. However, most common application ranges are between 1 to 4 MW for the power ratings, and 3.3 and 6.6kV for the voltage ratings. Approximately, 85% of the installed MV drive applications include fans, pumps, compressors and conveyors. [9].

VFDs comprise two main parts; a rectifier which converts ac input into dc output, and an inverter which converts dc input into three-phase ac output, adjustable in magnitude and frequency. Depending on the type of the rectifier, voltage source VFDs can be classified into two main groups; uncontrolled dc bus VFDs and controlled dc bus VFDs. Figure 26-a shows the conventional VFD with fixed dc voltage for 3-phase induction motors. With this type of VFDs, energy can be transferred only from the utility side to the motor, and harmonics generated by the rectifier could be significant for the ac supply side. Figure 26-b shows a VFD topology with a controllable dc voltage. In this topology, harmonic injection into the utility side can be reduced by using chopper. However, due to the diodes in rectifier, energy can only be transferred from the utility side to the motor. Figure 26-c shows a controllable dc voltage topology which has a low

input power factor. However, regeneration (energy is bi-directional) is possible with this topology [10].
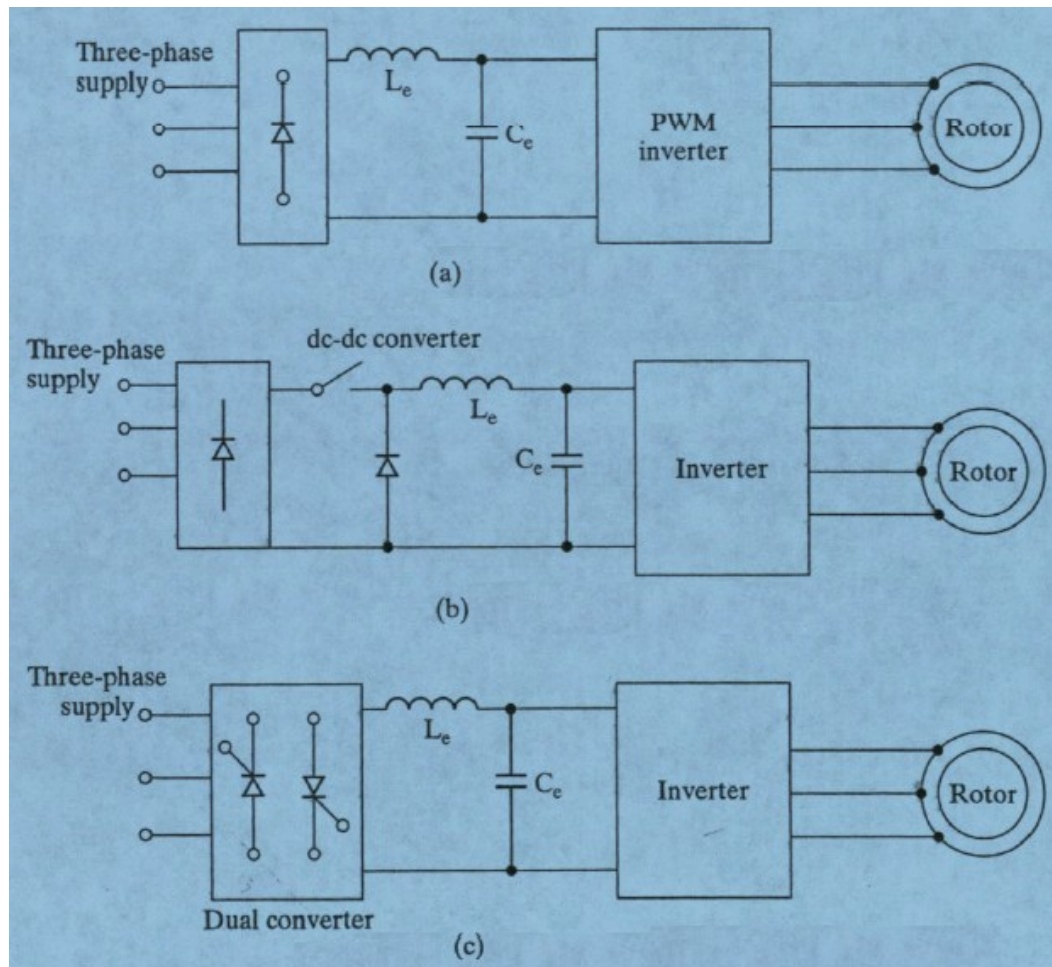
Figure 26: Voltage Source Induction Motor Drives [10]

Controlled rectifiers are used in some power electronics applications where a controlled dc voltage is necessary, such as battery chargers and dc motor drives. As it is mentioned previously, energy can be bi-directional in some topologies which can increase the efficiency of the entire system due to the allowance of regeneration.

Uncontrolled rectifiers are used in majority of the power electronics applications, such as ac motor drives, dc servo drives, switching dc power supplies, etc. Most of these applications do not include 60Hz bulky transformer, and the rectifier is directly connected to the utility [11]. However, due to the harmonic requirements set by North American and European standards such as IEEE Standard 519-1992, multi-pulse rectifiers are being used more and more as a front-end for high power drives.

3.1   Multi-pulse Diode (Uncontrolled DC Voltage) Rectifiers

The main purpose of multi-pulse rectifiers is to reduce the line current harmonic distortion by using a phase shifting transformer. 12-, 18-, 24-pulse or more pulse rectifiers can be configured by connecting each 6-pulse rectifier to one of the secondary windings of the phase shifting transformer. Due to the phase shifting between the windings of the transformer some of low-order harmonics caused by the six-pulse rectifiers are cancelled. Line current distortion decreases as the number of the pulses increases. Another use of phase shifting transformer is to block common mode voltages created by the rectifier and the inverter. The issue of common mode voltages is important for motors because it damages insulation on windings on motors, and cause early failure of winding insulation.

It is important to understand six-pulse rectifier before examining multi-pulse rectifiers. In Figure 27, a six-pulse rectifier is shown. The rectifier is supplied by a 3-phase voltage source, and output of the rectifier is shown as V_d.
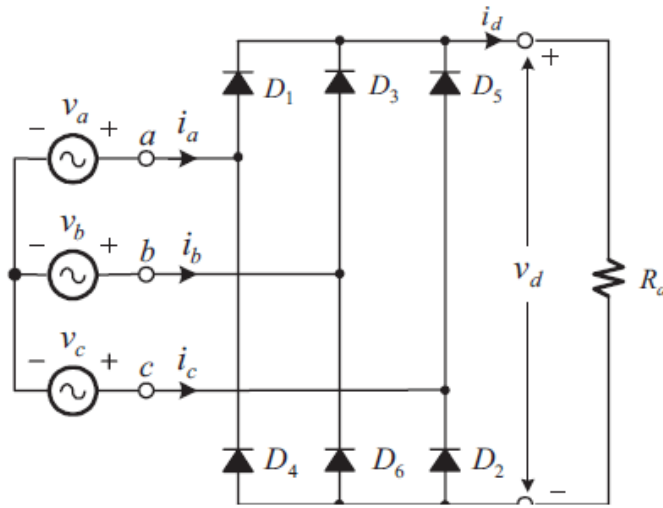
Figure 27: Six-pulse Rectifier Connected to a Resistive Load [2]

Waveforms of the six-pulse rectifier are shown in Figure 28. V_a, V_b, V_c are the phase voltages shown in Figure 27, and V_{ab}, V_{ac}, V_{bc} are phase-to-phase voltages which are shown in Figure 28. During the interval I, V_{ab} is higher than V_{ac} and V_{bc}, thus diodes 1 and 6 are turned on. Similarly, during interval II, V_{ac} is higher than other line-to-line voltages, thus diodes 1 and 2 are turned on, and during the next interval, V_{bc} is higher than the others, thus diodes 3 and 2 are turned on. The voltage seen on the resistive load becomes equal to the line-to-line voltages during relevant intervals, which are shown in Figure 28. Therefore, the dc voltage V_d seen on the resistive load has 6 pulses in one period of the supply frequency. The average of this voltage can be found by;

$$V_{do} = \frac{A_1}{\Pi/3} = \frac{1}{\Pi/3} \int_{\Pi/6}^{\Pi/2} V_{ab}(\omega t)d(\omega t) = \frac{1}{\Pi/3} \int_{\Pi/6}^{\Pi/2} \sqrt{2}V_{LL}\sin(\omega t + \Pi/6)d(\omega t) \approx 1.35V_{LL} \quad (3.1)$$

Here, V_{LL} is the rms value of the line-to-line voltage. Line currents can be calculated as dividing the dc voltage on the resistive load by the resistance value. As it is shown in

Figure 28, line currents have 2 humps in every half cycle of the line frequency. In Figure 28, only the current waveform of the phase-A, i_a, is shown. Other line currents, i_b and i_c have same waveforms but only they are lagging i_a by $2\pi/3$ and $4\pi/3$, respectively.
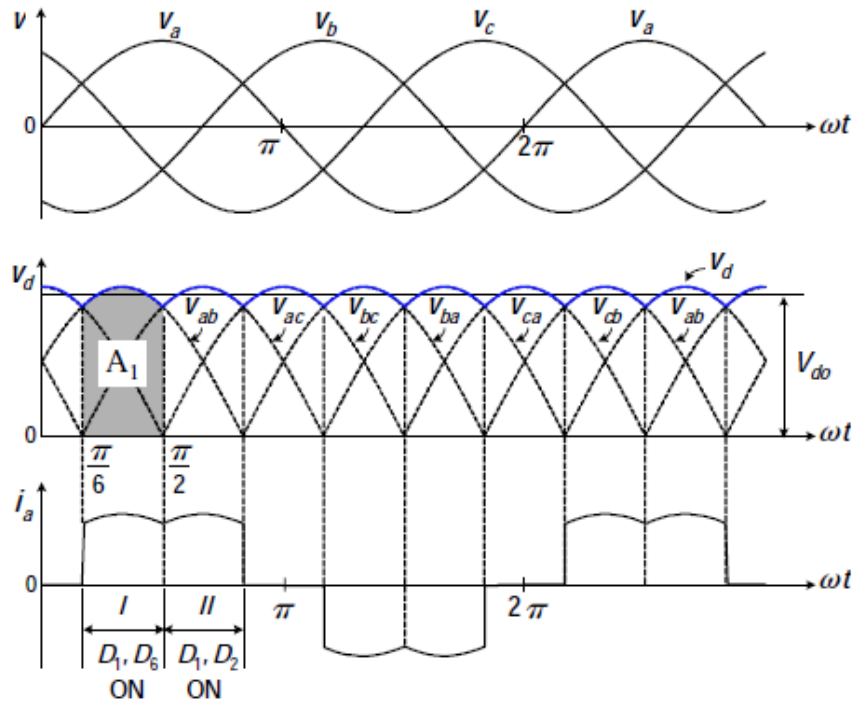
Figure 28: Waveform of the Six-pulse Rectifier (Resistive Load) [2]

It is obvious that line currents are periodical but not sinusoidal. Therefore, the waveform has some harmonics in it and total harmonic distortion can be calculated as;

$$THD = \frac{\sqrt{I_a^2 - I_{a1}^2}}{I_{a1}} \qquad (3.2)$$

where I_a is the rms value of the line current and I_{a1} is the rms value of the fundamental current. As the waveform becomes more like sinusoidal form, THD value decreases.

Due to the half-wave symmetry in the current waveform, there is no even order harmonics and no triplen (zero-sequence) harmonics since the three phase system is balanced. In general, 5th and 7th harmonics are dominant in the system, and they have higher magnitudes than other harmonics. Figure 29 shows the waveforms of two characteristic line currents drawn by a six-pulse rectifier.
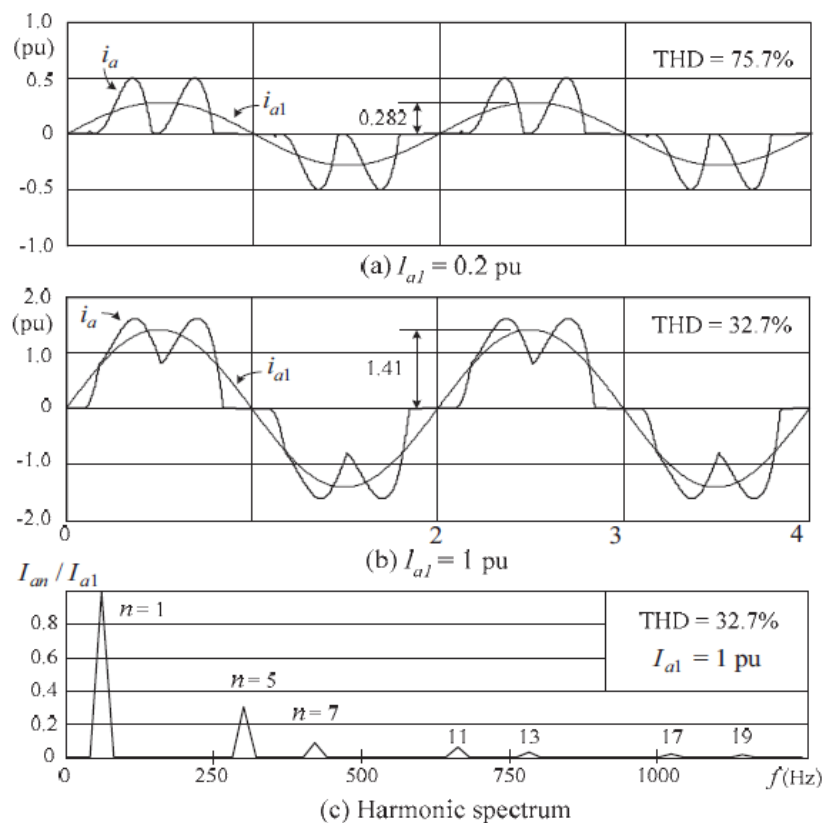
Figure 29: Waveforms and Harmonic Spectrum of a Six-pulse Rectifier [2]

It is clear that THD is 75.7% and 32.7% when the rms value of the fundamental current is 0.2 per unit and 1 per unit, respectively. This THD values are not within the limits set by North American and European standards such as IEEE Standard 519-1992.

Therefore, in order to meet the harmonic limitations, multi-pulse rectifiers are used as a front-end to VFDs.

3.1.1   Series Type Multi-pulse Diode Rectifier

It is stated earlier that, multi-pulse rectifiers consist of several six-pulse rectifiers connected to the secondary windings of a phase-shifting transformer. Series type diode rectifier consists of six-pulse rectifiers connected in series on the dc side. Therefore, for the medium-voltage drives, series type diode rectifier can only be used to supply inverter types which require one dc supply. Three-level neutral clamped (NPC) inverters and multilevel flying-capacitor inverters can be shown as an example to these inverters [2]

Figure 30-a, Figure 30-b, and Figure 30-c show typical topologies for 12-pulse, 18-pulse and 24-pulse series type diode rectifiers respectively. All six-pulse rectifiers are identical, and they are connected to the secondary windings of the phase shifting transformer. In order to eliminate lower harmonics in the line current, while one secondary winding is in phase with the primary winding, the other windings should have some phase difference with respect to the primary winding. Phase differences between the secondary windings are 30°, 20° and 15° for the 12-, 18- and 24-pulse rectifiers respectively as shown in Figure 30. Zigzag winding configuration is commonly used as secondary windings, and primary winding could be either Y or Δ-connected. Turn ratio of the transformer can be arranged according to the voltage requirements on the secondary sides.

The total leakage inductance of the transformer is shown as L_{lk}, and the total line inductance between the supply and the transformer is shown as L_s. A sufficiently large capacitor C_d is used to obtain ripple-free voltage V_d.

Assuming the multi-pulse rectifiers are operated under rated conditions with $L_s=0$ and a typical value of 0.05pu leakage inductance, an example of a 12-pulse rectifier waveforms are shown in Figure 31. As it is seen in the waveforms, the dc current i_d has 12 pulses per cycle of the supply frequency, and the line current of the Y-connected secondary winding i_a has a trapezoidal form with humps on top. The delta-connected secondary winding current $i_{\tilde{a}}$ has the same waveform except for 30° phase difference which is why not shown in waveforms.

The Y-connected secondary line current referred to the primary side is shown as i'_a, which has the same waveform with i_a because both primary and secondary windings are Y-connected. The only difference between waveforms is the magnitude change depending on the turn ratio. However, the waveform of $i'_{\tilde{a}}$, which is the delta-connected secondary winding current referred to the primary side, is different than waveform of $i_{\tilde{a}}$. The reason of this change in waveform $i'_{\tilde{a}}$ is due to the phase displacement of the harmonic currents during the referral from delta-connected secondary winding to Y-connected primary winding. As a result of this phase displacement, certain harmonics such as 5th and 7th are out of phase with those in i'_a, which results in cancellation of those in the primary line current of the transformer, given by,

$$i_A = i'_a + i'_{\tilde{a}} \qquad (3.3)$$

(a)

(b)

(c)
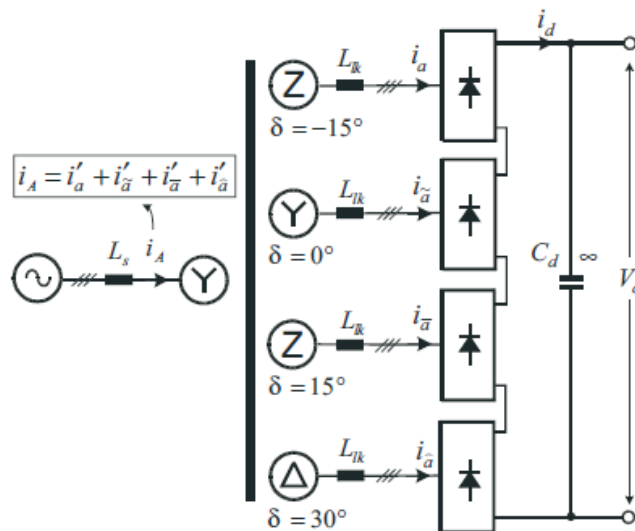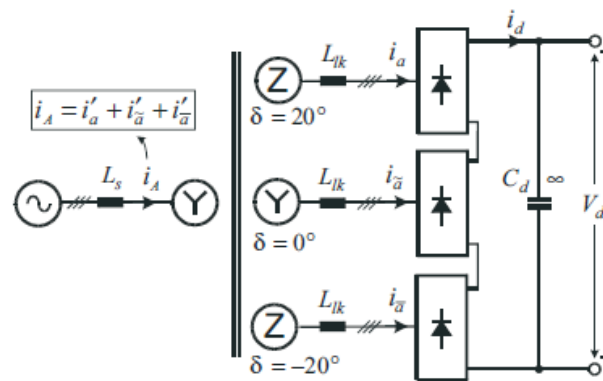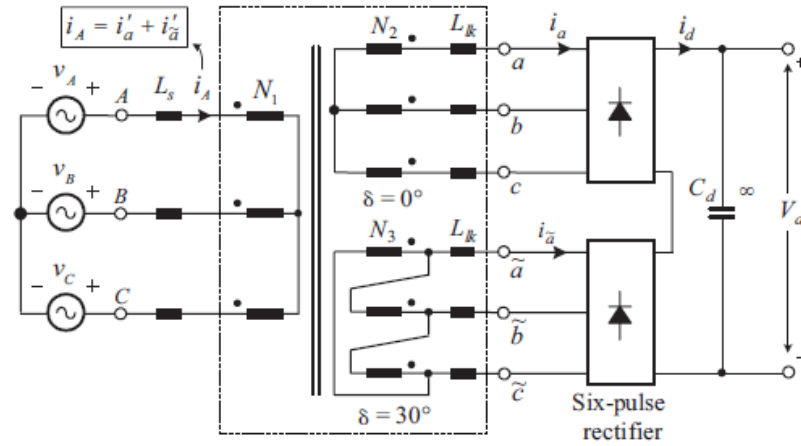
Figure 30: Series-type Diode Rectifiers

The harmonic contents of those secondary currents are same, resulting in same THD level which is around 24%. However, due to the displacement of those harmonic contents, they can cancel the most significant harmonics 5th and 7th in the current i_A whose THD level is lower and around 8-9% [2].
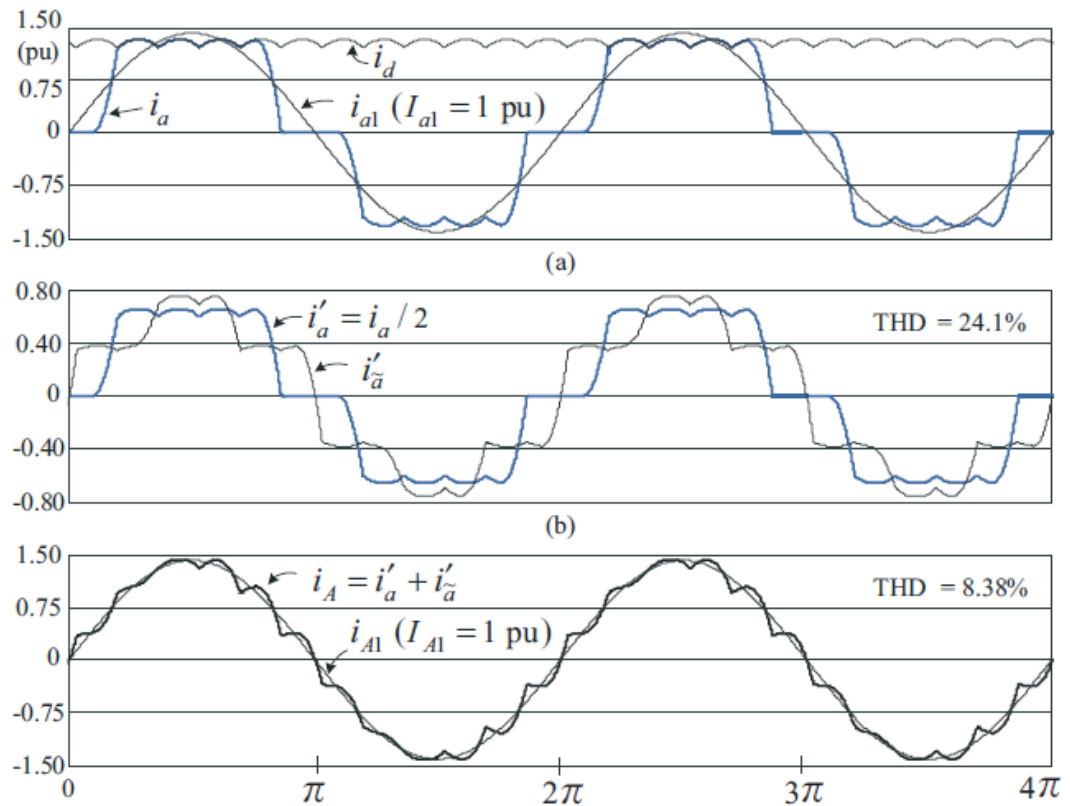
Figure 31: Current Waveforms of a 12-pulse Series-type Rectifier (L_s=0, L_{lk}=0.05pu, I_{A1}=1.0 pu)

This harmonic cancellation due to the phase shifting transformer is applied to the higher pulse-rectifiers in the same way. The phase angle between secondary windings of the 18-pulse rectifier is 20° and therefore, zigzag connection should be used in the

secondary windings. The proper phase angle between the secondary windings δ can be calculated as,

$$\delta = \frac{60^{o}}{\#\,of\,\sec ondary\quad windings} \qquad (3.4)$$

Therefore, the phase angle between secondary windings of 24-pulse rectifier is 15°. Since the whole idea is same for all of them, their waveforms are not given for those with more pulses. However, Table 2 shows an example of a system, and compares the THD levels for different multi-pulse rectifiers. It shows that while THD levels at the secondary side is the same, as the number of pulse increases, THD level at the primary side decreases.

Table 2: THD Levels of Multi-pulse Rectifiers

Rectifier Type	THD(%) at Secondary Windings	THD (%) at Primary Windings
12-pulse	24%	8-9%
18-pulse	24%	3-4%
24-pulse	24%	2%

3.1.2   Separate-Type Multi-pulse Diode Rectifier

Different than series-type multi-pulse rectifiers, separate type multi-pulse diode rectifiers supply separated dc loads. In other words, several inverters can be isolated from each other on the dc side by connecting to separate-type diode rectifiers. Multilevel

cascaded H-bridge inverter, which requires several isolated dc supplies, is a good example for usage of separate-type diode rectifiers. In Figure 32, an example of separate loads supplied by a 12-pulse separate-type diode rectifier is shown. The configuration of separate-type rectifier is the same as the series-type rectifier, except with separate-type rectifier, different loads can be supplied.
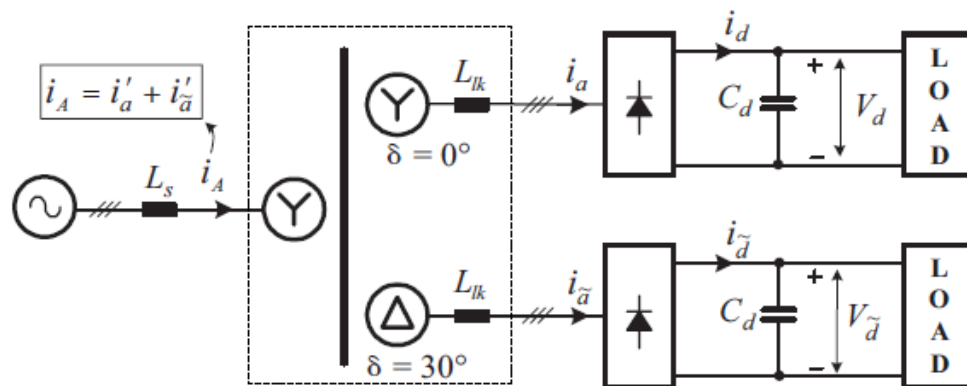
Figure 32: 12-pulse Separate-type Rectifier Configuration

Figure 33 shows an application of a 12-pulse separate-type rectifier which supplies a cascaded H-bridge multilevel inverter drive. In this application type, the phase shifting transformer has 6 identical secondary windings, and each of them feeds a six-pulse diode rectifier. Three of the windings are Y-connected with the angle $\delta=0^{\circ}$, and the other three windings are Δ-connected with the angle $\delta=30^{\circ}$. As it is obvious from the figure, one Y-connected and one Δ-connected windings feed two separate H-bridge inverters, which are cascaded on the output side. Those cascaded H-bridge inverters are connected to one phase of a 3-phase motor.
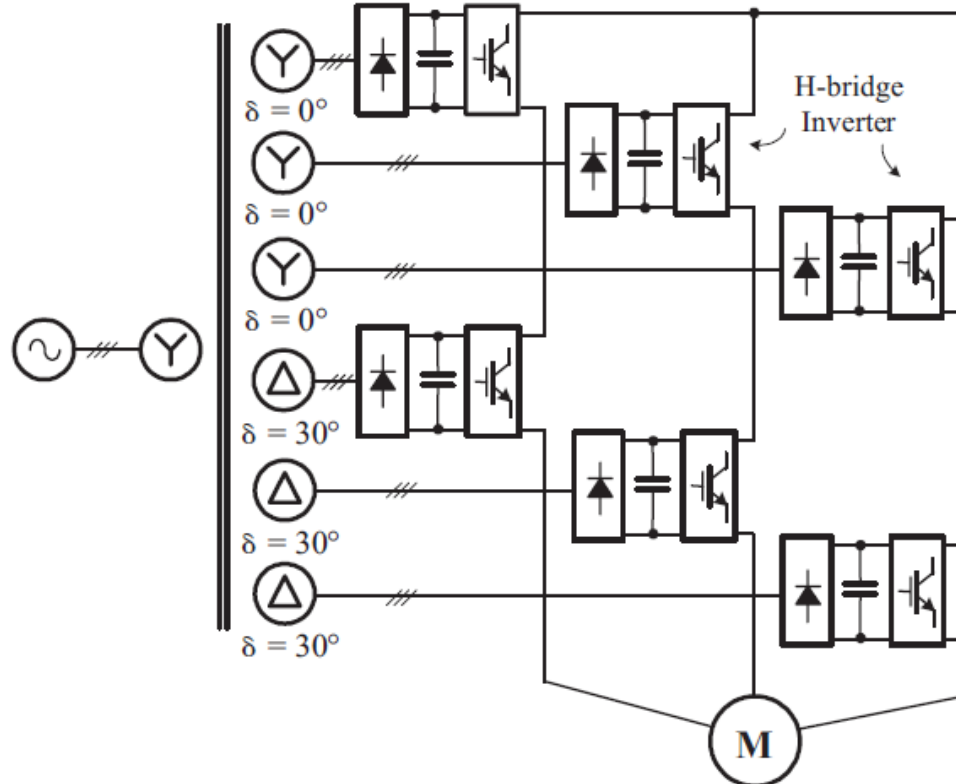
Figure 33: An Application of 12-pulse Separated-type Rectifier [2]

Figure 34 shows the waveforms of a 12-pulse separated-type rectifier connected to H-bridge inverters. The currents i'_a and $i'_{\bar{a}}$ are the referred secondary line currents to the primary windings. It is discussed earlier that 5th and 7th harmonics are cancelled due the displacement of these harmonics by phase-shifting transformer. Therefore, THD level of primary side (I_{An}/I_{A1}) is lower than secondary side THD level (I'_{an}/ I'_{a1}).
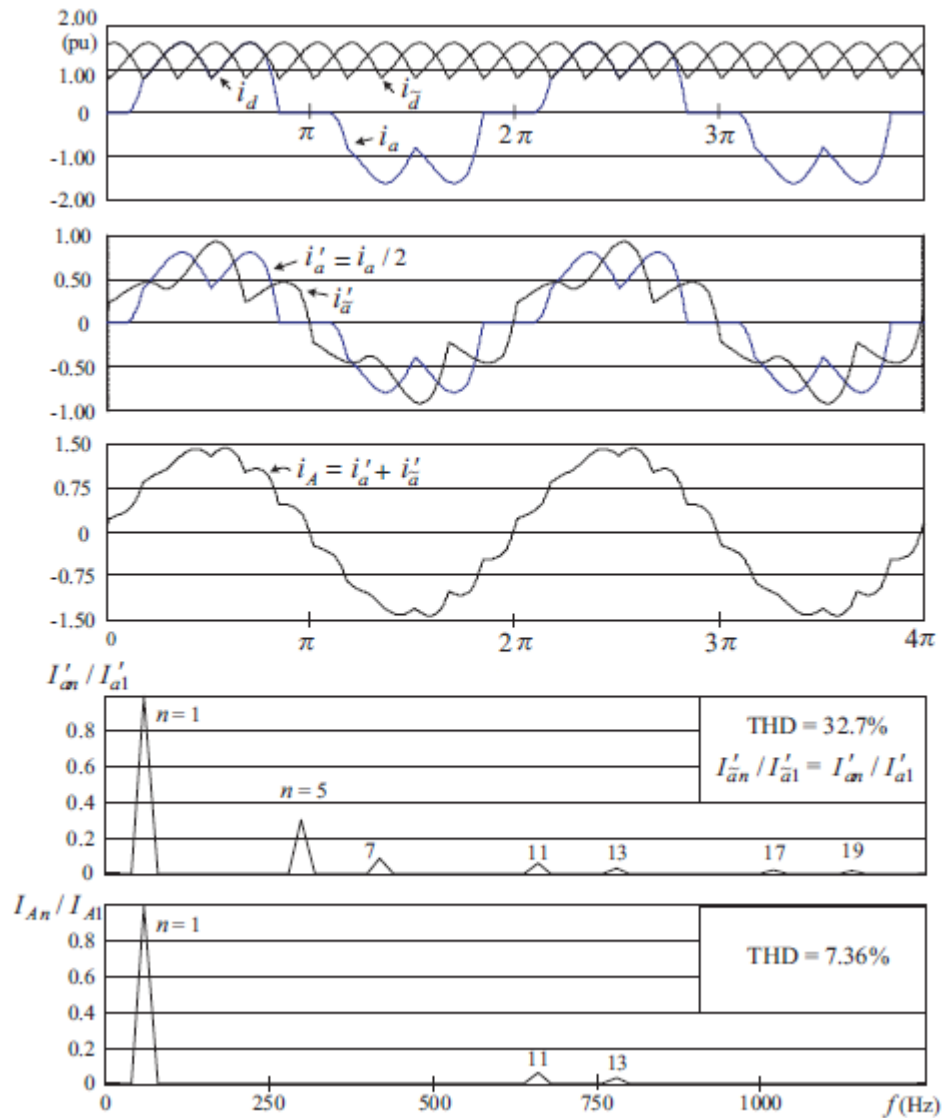
Figure 34: Current Waveforms of a 12-pulse Separate-type Rectifier ($L_s=0$, $L_{lk}=0.05$pu, and $I_{A1}=1.0$pu) [2]

If we compare Figure 34 with Figure 31(separate-type and series-type rectifiers), the primary side current waveforms (i_A) are very similar as well as the THD levels even the though secondary current waveforms are different than each other. This is because of the cancellation of the most significant harmonics 5th and 7th. The main difference is that, separate-type 12-pulse rectifier secondary line currents have lower 11th and 13th

harmonics and higher 5th and 7th harmonics than series-type 12 pulse-rectifier secondary line currents. When secondary currents are referred to the primary side, 5th and 7th harmonics are cancelled, thus separate-type rectifier has lower THD at the primary side than series-type rectifier due to the lower magnitude of 11th and 13th harmonics in separate-type rectifier.

Higher pulse separate-type rectifiers such as 18- and 24-pulse rectifiers have similar results. In 18-pulse rectifier due to the cancelation of 5th, 7th, 11th, and 13th harmonics, THD level is around 3% on the line side. Line side THD level becomes lower than 2% for 24-pulse separate-type rectifiers.

3.2   Multi-level Inverter Topologies

In recent years, as higher power equipments are needed more, focus on multi-level inverters has increased due to their significant advantages over traditional two-level inverters. Some of these advantages can be summarized as;

- Lower distortion on input current

- Higher power quality waveforms

- Reduced dv/dt stress

- Lower electromagnetic compatibility concerns

- Low switching frequency and low switching losses

- Smaller Common Mode (CM) voltage

- Excellent harmonic performance

- Staircase waveform voltage output and higher output voltage with lower stress on power switches.

Due to all these advantages, voltage-source multilevel inverters are highly popular, and can be mainly categorized into three main groups; cascaded H-bridge inverters, diode-clamped inverters, and capacitor clamped inverters.

3.2.1 Cascaded H-Bridge Multilevel Inverters

Cascaded H-bridge (CHB) multilevel inverters, which consist of several single phase H-bridge power cells, is one of the most common medium voltage (MV) source drives. Each H-bridge power cells are fed by an isolated dc supply, which is generally provided by multi-pulse separate-type diode rectifiers. H-bridge power cells are cascade connected on their ac-side, and the number of cells are determined according to the operating voltage level.

In Figure 35, a typical multilevel cascaded H-bridge inverter for a VFD (Variable Speed Drive) topology is shown. Each H-bridge cell generates 3-level output ($\pm V_{dc}$, 0V), and with this inverter topology consisting of 4 H-bridges on each phase leg of the induction machine, it is possible to generate 9 levels of output phase voltage (inverter phase voltage, V_{AN}), therefore it is called 9-level H-bridge topology. If H is the number of the H-bridge cells per phase leg, then the number of the voltage levels (m) in a CHB inverter can be calculated as [2];

$$m = 2H + 1 \qquad\qquad (3.5)$$
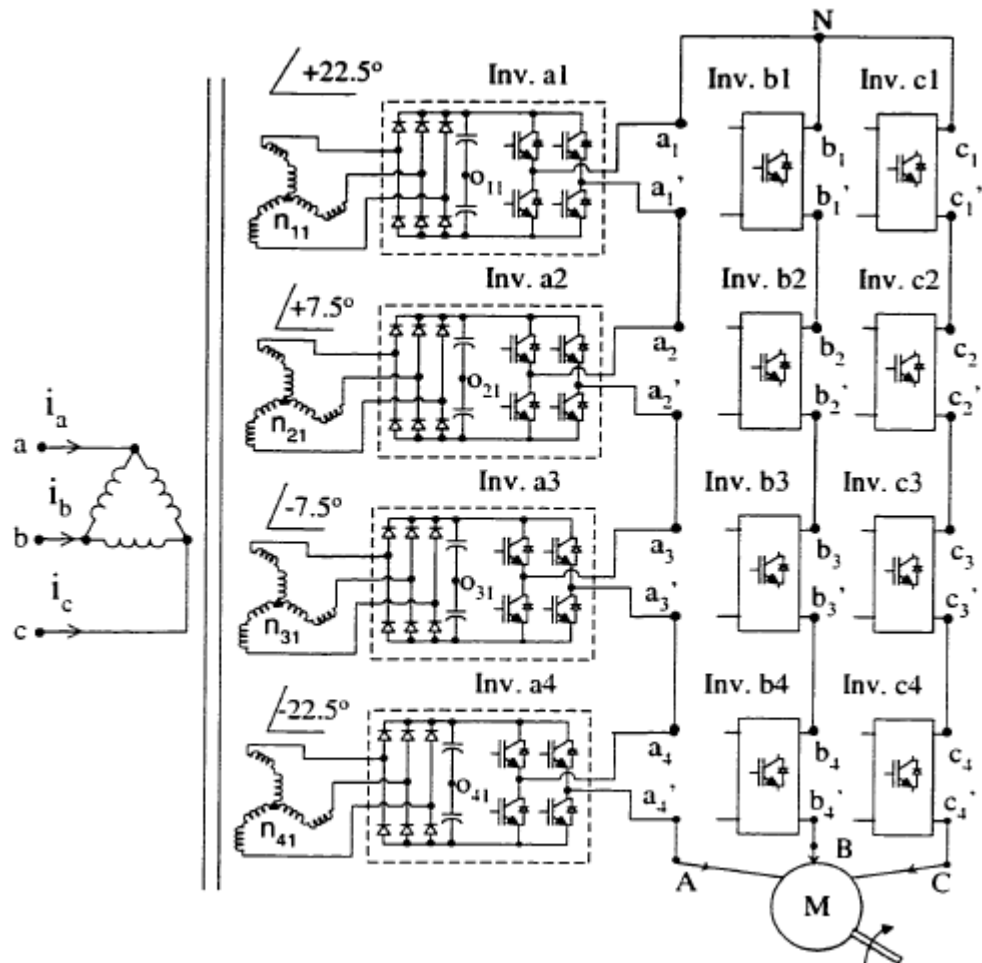
Figure 35: A Multilevel Separated-type Rectifier fed Cascaded H-bridge Inverter used in an ASD Topology [12]

Each H-bridge inverter cell is fed by generally fixed dc voltage, and output voltage of the inverter can be adjusted by Pulse Width Modulation (PWM) schemes which are explained in the following section.

There are several advantages of cascaded H-bridge (CHB) inverters; some of these are;

- Due to the phase shifting input transformer, utility input current is clean.

- Due to the identical modular structure, manufacturing and maintenance costs are low. Easily available lower voltage IGBT devices are used.

- The motor terminal voltage has several small steps which are equal to the dc-bus voltage of a single-phase inverter. Therefore, the need for dv/dt filter is eliminated, and harmonic content of the motor terminal voltage is lowered.

- Any output voltage can be generated simply by cascading the H-bridge cells. Thus, high voltages can be obtained due to the flexible structure, and there is no equal-voltage sharing problem on the series-connected devices.

- A fault on an H-bridge cell does not require shut-down of the whole system.

3.2.1.1 Pulse Width Modulation

Pulse Width Modulation (PWM) technique normally requires a sinusoidal modulating wave and a triangular carrier wave. By comparing these two waves, signals to the switches (S_1, S_2, S_3, S_4) shown in Figure 36 are produced. On the same leg, upper and lower switches are not both turned-on or –off at the same time. In other words, on the same leg while the upper switch is turned on, the lower switch is turned off. Therefore, one gate signal for each leg- two for the H-bridge inverter- is enough to operate the inverter.
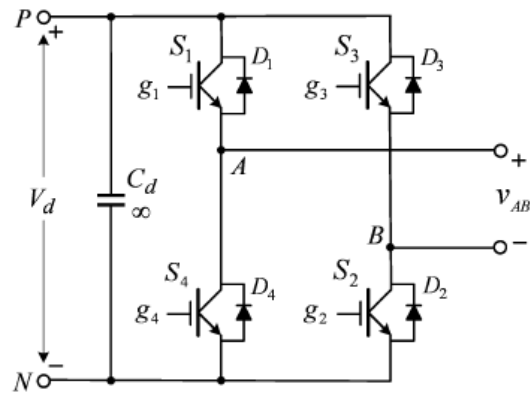
Figure 36: Single-phase H-bridge Inverter [2]

As it is mentioned before, dc input voltage to an H-bridge inverter shown as V_d in Figure 36 is generally fixed. The output voltage V_{AB} can be adjusted by bipolar or unipolar pulse width modulation technique. Figure 37 shows the waveforms of an H-bridge inverter controlled by bipolar PWM technique. Here, V_{cr} and V_m are carrier and modulation voltage waves, respectively. Frequency of the carrier wave is 900Hz, and modulation wave frequency is 60Hz. Thus, the frequency modulation index ($m_f = f_{cr} / f_m$) becomes 15, and amplitude modulation index ($m_a = V_{m\_peak} / V_{cr\_peak}$) is selected as 0.8. Depending on the gate signals, the output voltage of the H-bridge cell V_{AB}, which varies between negative and positive value of V_d (bipolar modulation), is shown in Figure 37. Normalized harmonic spectrum of the output voltage is shown in Figure 37. The spectrum shows the RMS value of the harmonics, and these harmonics are concentrated around the modulation index m_f and its multiples for bipolar pulse-width modulation technique. Here, the switching frequency seen by the load is equal to the carrier frequency which is 900Hz.
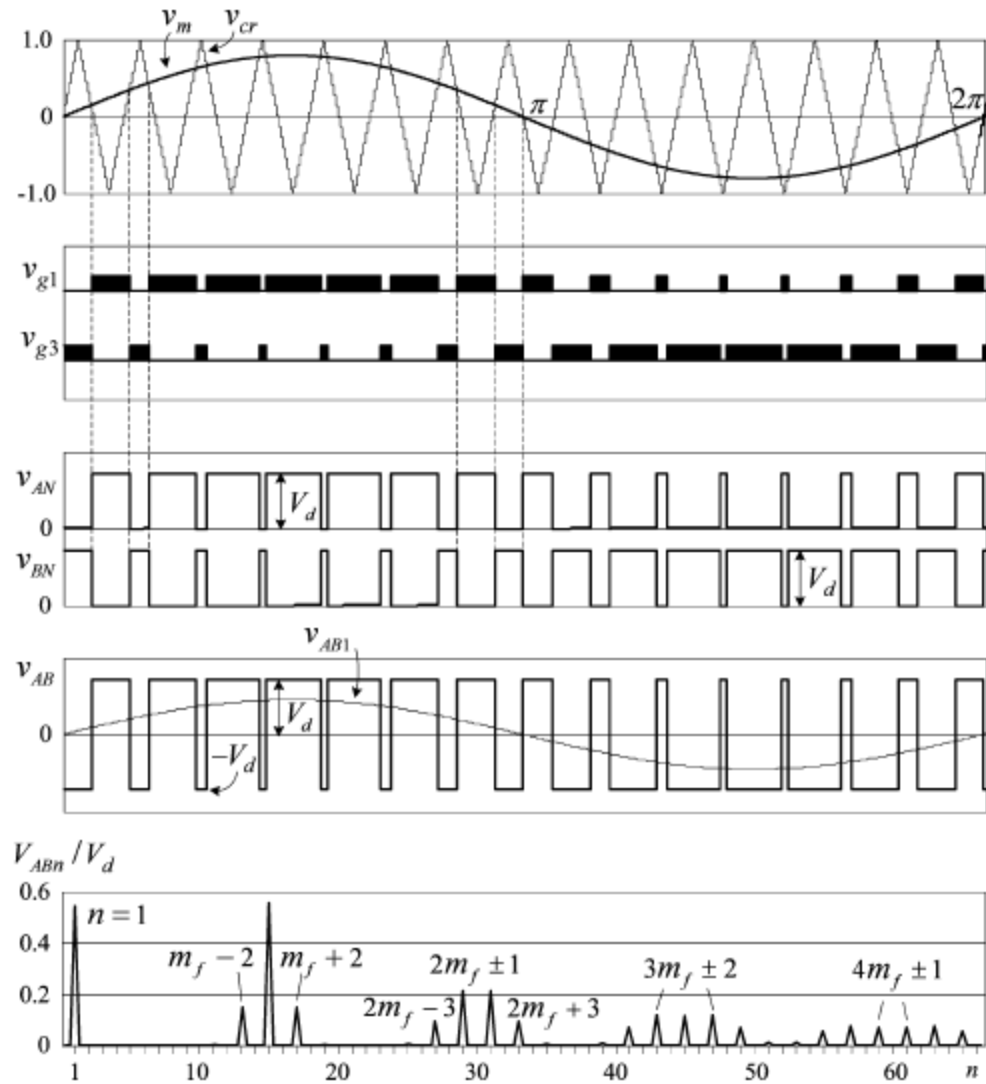
Figure 37: Bipolar PWM Waveforms for an H-bridge Inverter [2]

The unipolar PWM technique is shown in Figure 38. Different than bipolar PWM technique, either two modulation sinusoidal waves or two carrier waves are required to generate the gate signals in this method. The modulation waveform shown in Figure 38 as V_{m-} has the same frequency and magnitude with the waveform V_m, yet $180°$ phase shifted. Similar with the bipolar PWM, the output voltage waveform is produced depending on the gate signals. This time, the output waveform is changing between V_d

and zero during the positive half cycle, and between zero and $-V_d$ during the negative half cycle. Therefore, it is called unipolar PWM technique. The normalized harmonic spectrum is shown in Figure 38, and harmonics are centered around $2m_f$ and $4m_f$ this time. The harmonics around the frequency modulation index m_f are eliminated by unipolar modulation. In this type of modulation, the load "sees" $2m_f$ as a switching frequency.
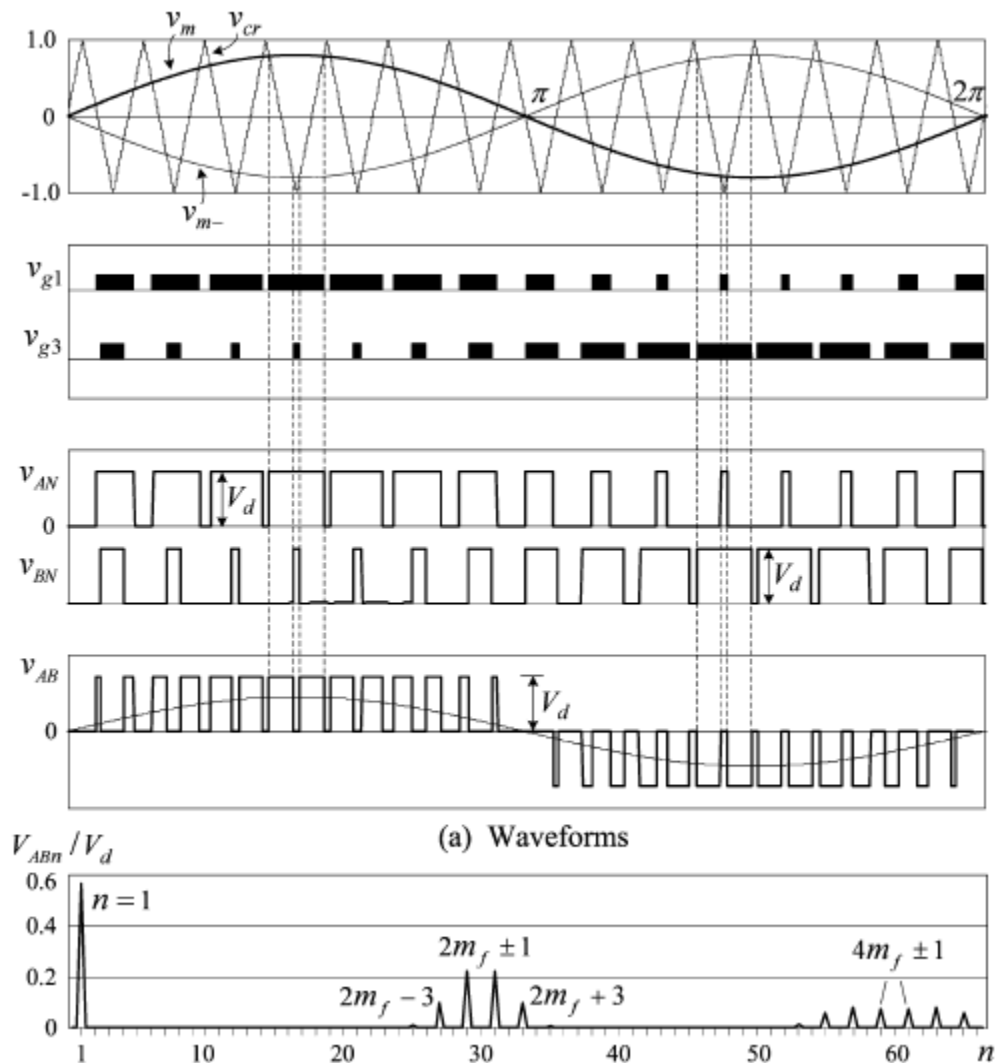
Figure 38: Unipolar PWM Waveforms for an H-bridge Inverter [2]

3.2.2 Diode-Clamped Multilevel Inverter

Diode-clamped multilevel inverters consist of clamped diodes and cascaded dc capacitors in order to obtain multilevel ac output waveforms. Although the converter can be configured as a three-, four- and five-level topology, only three-level topology is being used commonly in high power medium voltage drives. This special, three-level topology is often called as neutral-point clamped (NPC) inverter.

Figure 39 shows the simple form of a three-level diode-clamped inverter (NPC). Each leg of the inverter has four switching elements. Two dc bus capacitors are used in order to obtain a middle point Z which is called neutral point. The diodes D_{Z1} and D_{Z2} are called clamping diodes.
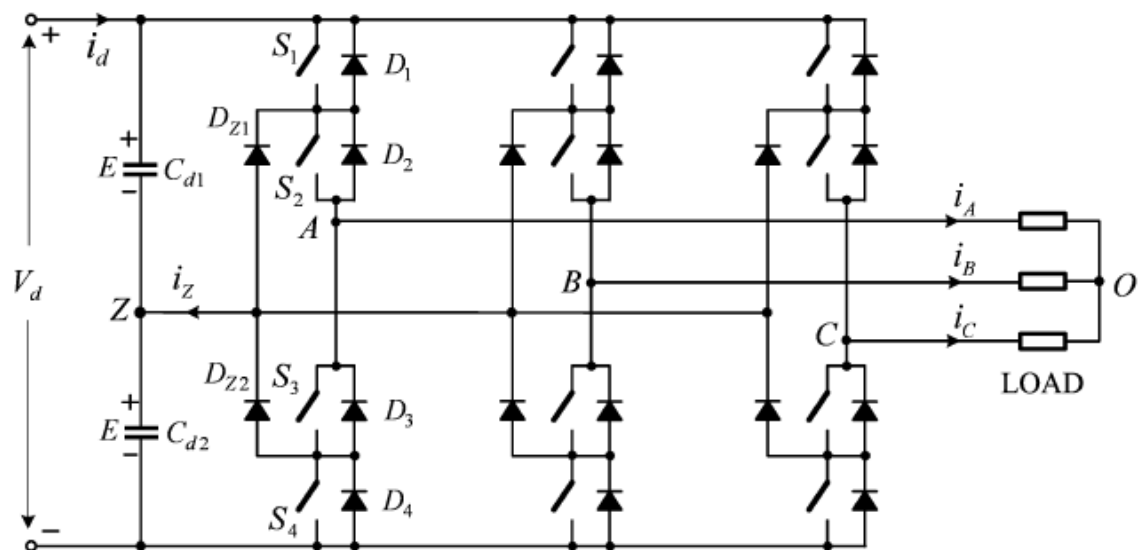
Figure 39: Three-level NPC Inverter [2]

In Figure 40, a VFD topology with a neutral-point clamped inverter is shown. The inverter is connected to a 12-pulse diode rectifier through a dc-link. As it is explained earlier, the inverter produces three-level phase voltage on the output side, and five-level motor terminal voltage. In order to obtain these voltage levels, switching operations should be arranged. Table 3 shows an example for producing three-level phase voltages. S_1, S_2, S_3, and S_4 are the switches, and E is the voltage across the capacitors shown in Figure 39.
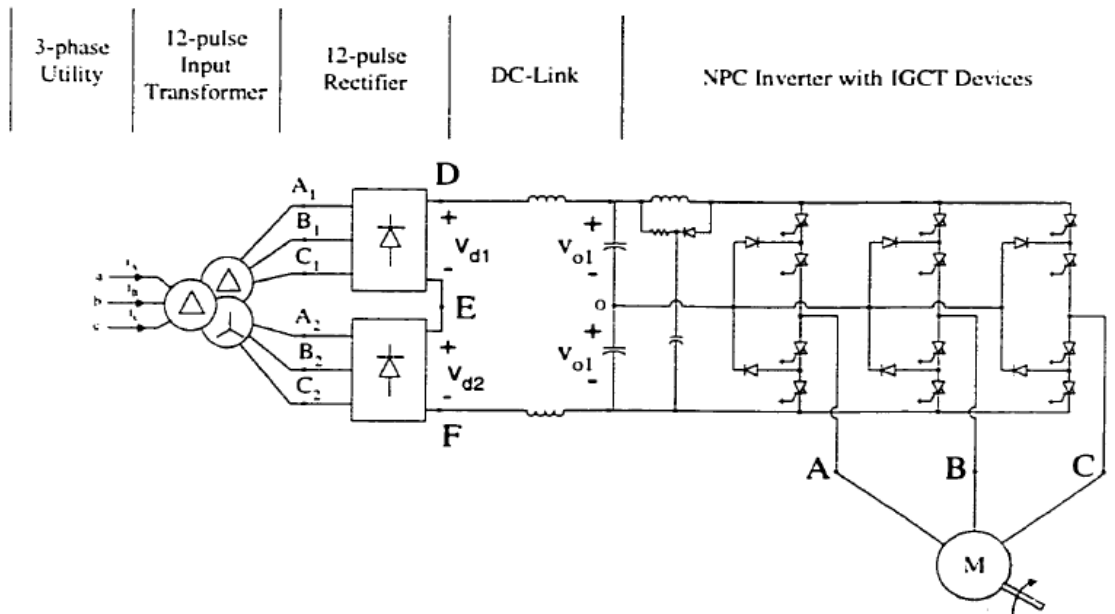
Figure 40: A VFD Topology using NPC Inverter [12]

Table 3: Switching States

Switching State	Device Switching Status (Phase A)				Phase Voltage
	S_1	S_2	S_3	S_4	V_{AZ}
P	On	On	Off	Off	E
O	Off	On	On	Off	0
N	Off	Off	On	On	E

In general, the NPC inverter can be used in high power applications, and it has the advantage of having the five-level motor terminal voltage which leads lower harmonic contents. The other advantage of the NPC inverter is that, each switching element has to support only half of the dc-bus voltage and needs to be able to block dc-bus voltage.

The main disadvantage of the NPC inverter for medium voltage applications is the need for dv/dt filtering at the output of the inverter. Due to the high dc bus voltage, high voltage insulation is needed within the VFD. Moreover, the NPC inverter is not modular; therefore the maintenance is not easy. Another disadvantage for the NPC inverters is the common-mode voltage (zero-sequence voltage), which curtails the insulation of motors.

3.2.3   Flying-Capacitor (Capacitor clamped) Inverter

Flying-capacitor inverters are another type of configuration of multilevel inverters. This configuration is modified by adding dc capacitors to the cascaded switches. Figure 41 shows a five-level capacitor clamped inverter configuration. S_1 and S'_1, S_2 and S'_2, S_3 and S'_3, S_4 and S'_4 are complementary switches; therefore four gate signals per leg are needed to operate the inverter. Five different phase and nine line-to-line voltage levels can be obtained by different sets of switching. Each switch needs to withstand the voltage across one of the capacitors. Eighteen capacitors are necessary for

a five-level capacitor clamped inverter. This large capacitive storage provides an advantage to capacitor clamped inverter during power outages.
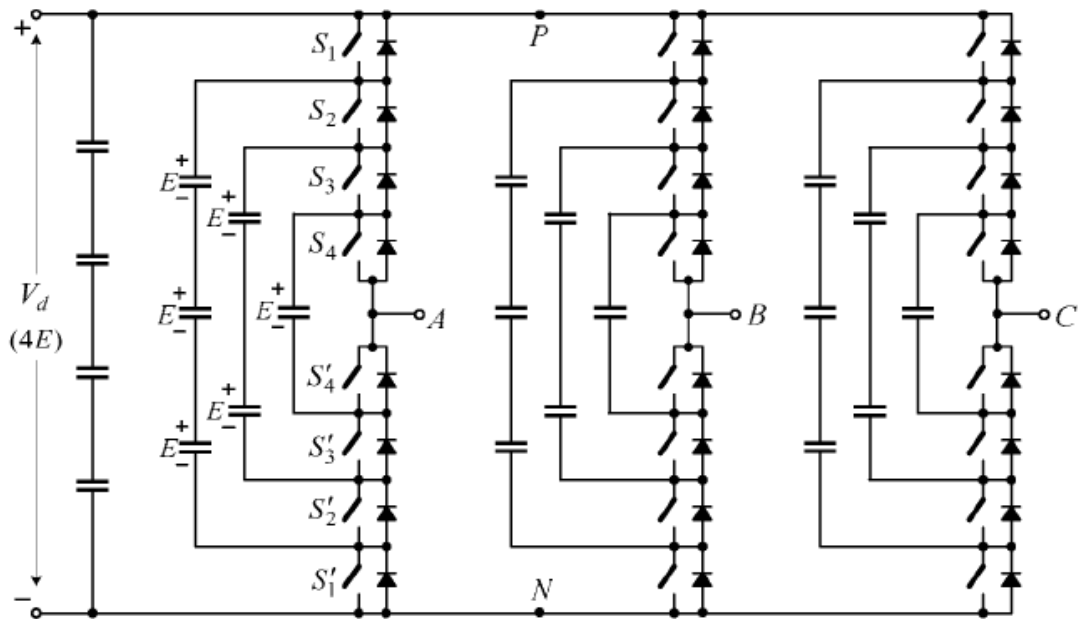
Figure 41: Five-level Capacitor Clamped Inverter [2]

As the output level of the capacitor clamped inverter increases, there is a quadratic increase in the number of the needed capacitors with their separate pre-charge units. For high output levels, the system becomes impractical due to the large number of the capacitors. Another disadvantage of this inverter is the difficulty in balancing the capacitor voltages. The voltage control on the flying capacitors should be done carefully in order to avoid the dc voltage deviation. Further, due to the inequality in the conduction periods of the switches, the current ratings of the devices are different. This is a disadvantage in terms of complexity in gate drive circuits [12]. Applications of

capacitor-clamped inverters are limited for drive systems due to the drawbacks mentioned.

3.3 Comparison of the Multi-level Inverter Topologies

Table 4 summarizes the comparison of the multilevel inverter topologies. For all of these multilevel inverter topologies, due to the increased level of output voltage, dv/dt and THD are lower compared with the conventional, two level inverter topology. However, each topology has its own advantages and drawbacks depending on their topology needs. The user should consider the motor and the system requirements in order to decide on the inverter topology for the required motor drive.

Table 4: Comparison of Multilevel Inverter Topologies

Multi-level Inverter Type	Advantages	Disadvantages
H-bridge	- Modular(easy maintenance &cheap) - Scalable after installation for different power and voltage rates - Redundant switching allows higher reliability in case of a switch failure - No switching devices in series - Allows lower rated switching devices - No voltage unbalance problem - Low THD - Low dv/dt	- Requires separate dc sources.(bulky, expensive, phase-shifting transformer needed) - Large number of switching devices(mostly IGBTs)
Diode Clamped	- Allows group capacitor charging - High efficiency for fundamental frequency switching - Low THD - Low dv/dt	- Not modular - Not scalable after installation - Large number of clamping diodes - Difficulty for higher than three-level output - Possible deviation of the neural point voltage - Entire system failure in case of a switch failure
Capacitor Clamped	- Allows system run through voltage sags and short power outages - Allows real& reactive power control	- Not modular - Bulky capacitors - Large number of capacitors - Separate pre-charging unit for each capacitor - Complex control for capacitor voltage balance - Entire system failure in case of a switch failure - Poor efficiency

4. SYSTEM COMPONENTS AND SIMULATION RESULTS

The general arrangement of the simulated system is shown in Figure 42. The simulation tool PLECS is used to simulate the system. The simulations are done under the assumption of a balanced 3-phase system. The focus of the simulations will be on the motor side of the system.
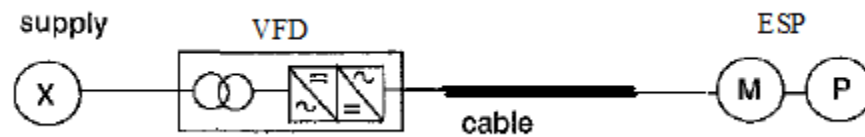
Figure 42: Schematics of VFD Drive System

The nominal voltage of the system is 11kV. The cell voltage in VFD is set as 690V. Switching frequency is 900Hz (m_f=15) and amplitude modulation index is 0.8.

4.1 System Components

A 36-pulse, multilevel variable frequency drive, an umbilical cable, and an ESP motor form the power system for offshore platforms shown in Figure 42. The details about the components are given in the following.

4.1.1   Subsea Cable

General Cable Exzhellent XXI designed for 20kV is picked as the subsea cable for the simulation. The datasheet of the cable is given in Appendix A. The cable has $1\times150\text{mm}^2$ conductor which has about 15 mm diameter and a metallic screen which is grounded, and XLPE insulation around. The overall diameter over the sheath is about 36mm. The maximum conductor DC resistance is 0.124Ω/km, star reactance per phase at 50Hz is 0.115Ω/km, and capacitance per phase is 0.252μF/km. The cross-section of the cable is given in Figure 43.
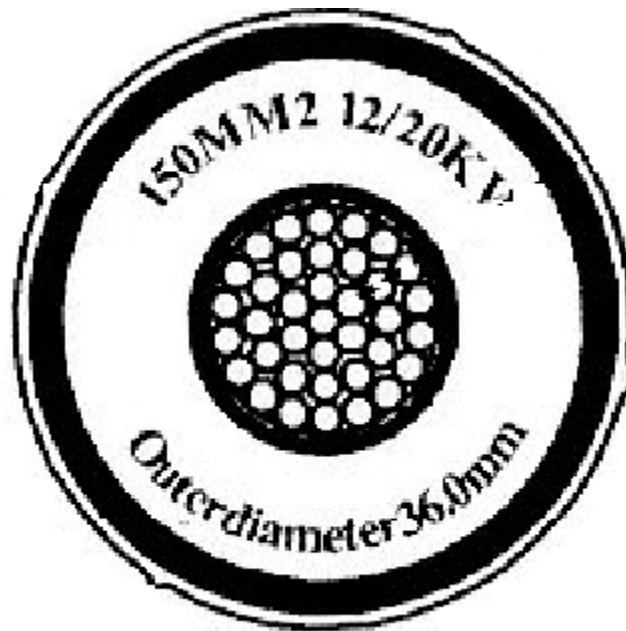
Figure 43: Cross-section of General Cable-Exzhellent XXI

Figure 44 shows the cross-section of an umbilical cable which consists of 9 General Cable - Exzhellent XXI, shown in Figure 43. Generally, umbilical cables

include two or three 3-phase cables so that with one umbilical cable, two or three separate circuits could be supplied. In the simulations, only one three-phase of this umbilical cable is energized and the others are used as spare. Therefore, there is no effect from adjacent circuits. However, if more than one 3-phase circuit is energized, there might be imbalances in voltage, thus may result in torque pulsations. This study is left as a future work.
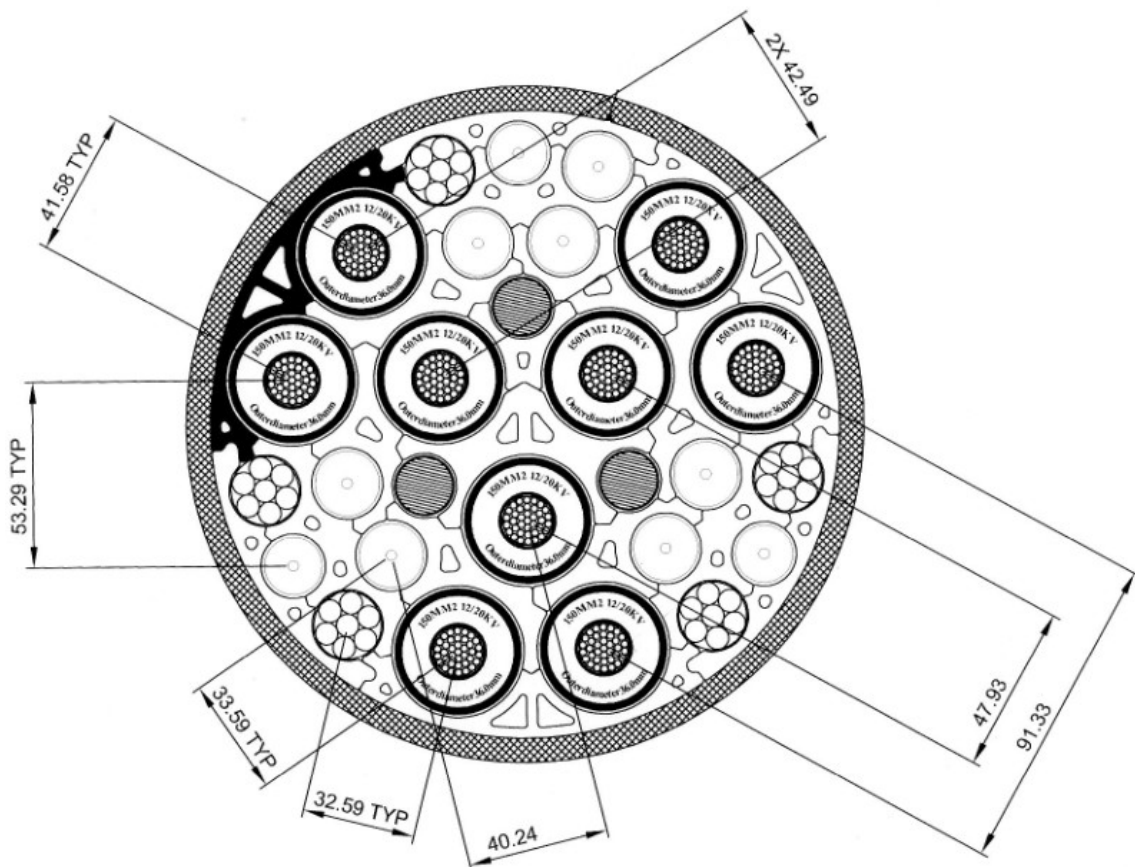
Figure 44: The Umbilical Cable

In chapter 2, Π-model and the frequency analysis of General Cable-Exzhellent XXI including the skin effect is given. Therefore, the calculations will not be repeated here. The same parameters are used in the simulations.

4.1.2 VFD

Siemens Rabicon Perfect Harmony is selected as a variable frequency drive for the simulations. It is a 36-pulse voltage source H-bridge variable frequency drive (VFD) with 690V cell voltage (dc-bus voltage). Its supply voltage is 11kV, maximum output voltage is 7200V, output frequency range is 0-60Hz, and it can run through up to 30% voltage dip. Datasheet of the VFD is given in Appendix B. Figure 45 shows the diagram of the VFD and the rest of the system. As it is seen in the figure, on each phase to the motor, there are multiple power cells connected in series on the output side of the VFD. Output of each cell can be controlled individually by pulse width modulation (PWM) technique which will be explained in the following.

As it is explained in chapter 3, each cell has a rectifier, a smoothing filter (capacitor) and an inverter. Inputs of the rectifiers are supplied by the secondary of a phase shifting transformer in order to reduce the harmonic distortion on the line side of the transformer. Extended delta windings or zigzag windings can be used as secondary windings. The secondary windings of the phase shifting transformer are phase shifted with respect to the primary winding. The phase shift can be calculated as [13];

$$PhaseShift = \frac{60}{\#cells \, / \, phase}$$

(4.1)

Phase shift for a 36-pulse drive should be 10°.

After rectification, dc voltage is converted to ac voltage by PWM inverter in each power cell. The cell voltage is 690V, thus all power cells consist of low voltage components. By having series connection at the output of the cells, medium voltages can be achieved. Each cell is controlled by separated PWM scheme. Mostly IGBTs are used as switching elements. Phase shifted multi carrier modulation scheme is used to produce ac voltage on the output side of the power cells. In this method, a sinusoidal reference signal (modulation signal) at the output frequency and triangular carrier signals at the switching frequency, which are identical except phase shifted, are produced for each power cell in phase A. Phase shifts between adjacent carrier signals in phase A can be calculated as [2];

$$\phi_{carrier} = \frac{360^o}{m-1}$$

(4.2)

where m is the voltage level of the inverter. The voltage level for an H-bridge inverter can be calculated by (3.5). For a 36 pulse drive, there are 13 levels of voltage, thus carriers on the same leg (phase A) should be shifted by 30° from each other. By comparing triangular carrier signal with the reference signal, gate signals to the switches are produced. When the reference signal is higher than the carrier signal, the signal to the left leg of the inverter is on, turning on the upper switch and off the lower switch. When the reference signal is greater than the inverse of the same carrier signal, then right leg signal becomes on, turning on the upper switch and off the lower one. This cycle is same
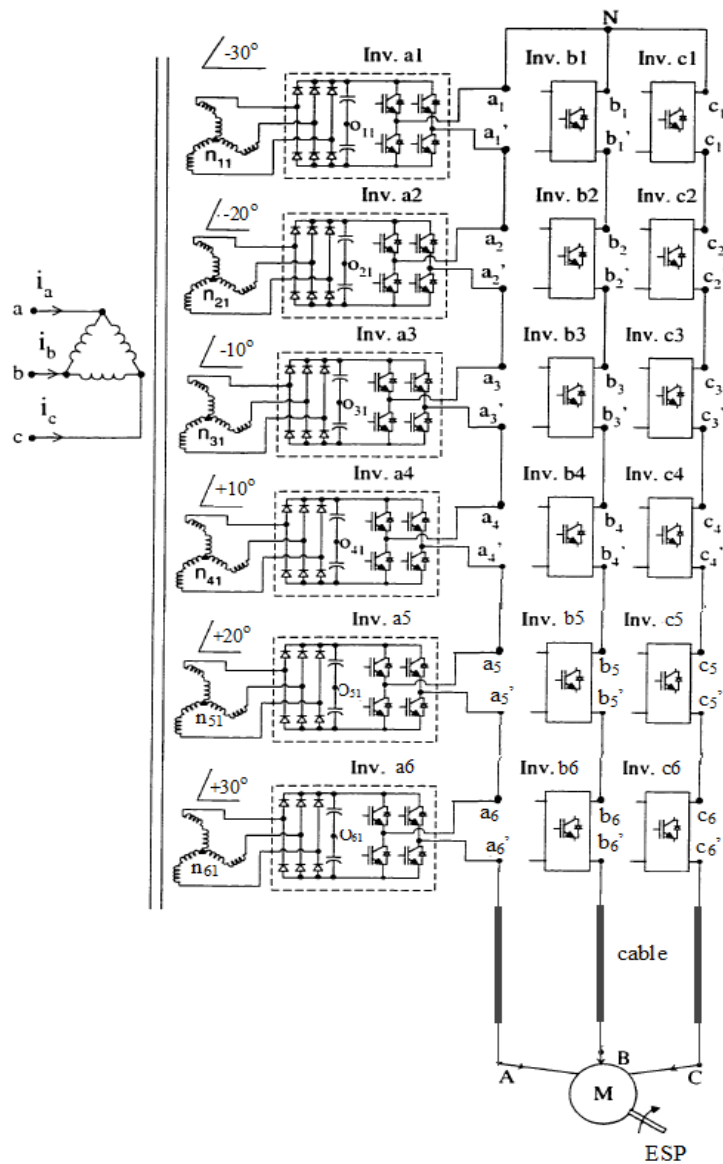
Figure 45: Diagram of the 36-pulse VFD

for each power cell, except that the carrier signals are shifted as explained before. Phase

B and Phase C have the same methodology except all the signals are phase shifted by

120° and 240°, respectively. In the simulations, the carrier frequency is picked as

900Hz, and that amplitude modulation index ($m_a = V_{m\_peak} / V_{cr\_peak}$) is set as 0.8. Since

the simulations are done under the assumption of steady-state condition, and there is no

feed-back control in the system, the frequency of the reference signal is equal to the system frequency which is 60Hz.

4.1.3   ESP Motor

An electrical submersible pump (ESP) system is a sealed device that includes an electric motor and a centrifugal pump coupled together. The kinetic energy from the motor produces great centrifugal motion in the pump forcing oil up to the surface. Electric submersible pumps are preferred for offshore oil applications due to the space limitations, and are generally vertically submerged in oil. Figure 46 shows an ESP installation on the seabed. The main disadvantage of an ESP system is that low mass oil flow will cause overheating in the system, curtailing the winding insulation of the motor.

A 850HP ESP motor by Baker Hughes is selected for the simulations. The nominal terminal voltage of the motor is 4239V and the maximum terminal voltage is 4493V. Minimum motor terminal starting voltage is 1696V and full load current is 120A. The data sheet of the motor is given in Appendix C. In Figure 47, the per phase equivalent circuit of the motor is given. Table 5 shows the parameters R_1, R_2, X_1, X_2 and slip at the full load for 36F^o. The simulations are done for full loading condition at the steady state. Two motors connected in parallel used for the simulations. The motors are star connected, and there is no feed-back control in the system.
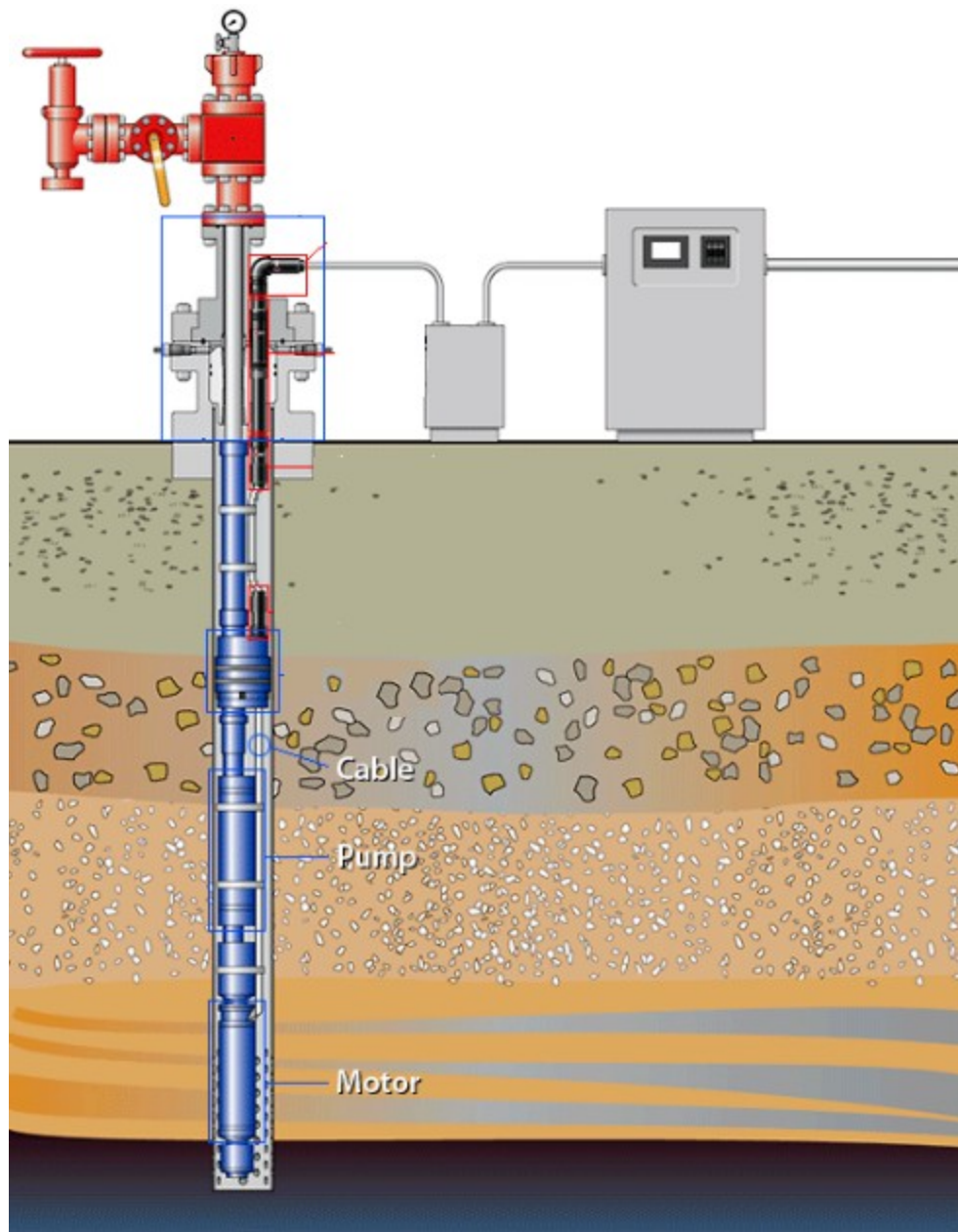
Figure 46: An ESP System Installation on the Seabed
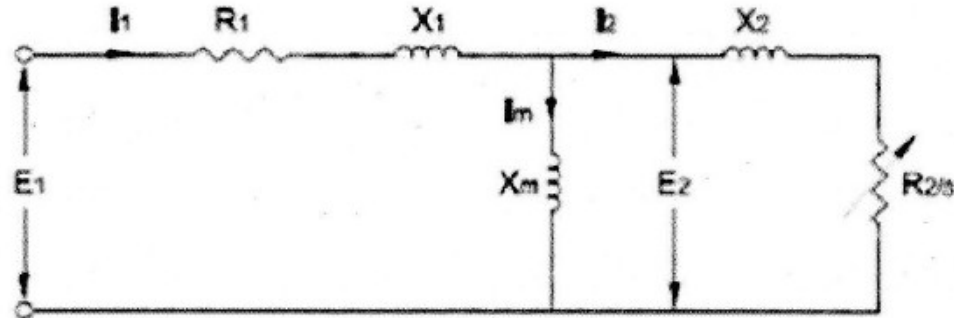
Figure 47: Per Phase Equivalent Circuit of the Motor

Table 5: Motor Per Phase Equivalent Circuit Parameters at 60Hz

Parameter	@36F°	@250F°
R_1	0.5280Ω	0.7376 Ω
X_1	3.4032 Ω	3.4032 Ω
X_m	65.2272 Ω	65.6656 Ω
R_2	0.7072 Ω	0.9568 Ω
X_2	3.7088 Ω	3.7232 Ω
Slip(s)	0.0322	0.0439

4.2   Simulation Results

In the results, the waveforms are represented by the following abbreviations;

- V_AO_motor→motor phase voltage

- V_AB_motor→motor phase-to-phase voltage

- V_AB_VFD→VFD phase-to-phase output voltage

Motor terminal voltages for different cases will be compared. The effect of the umbilical cable on the motor terminal voltages will be shown. By using high frequency modeling of the cable, high frequency effect of the VFDs on ESP system will be analyzed. In all cases, total current harmonic distortion of the motors are much lower than 1%, therefore current values are not included. In the following, seven different case results are given, and the discussions are done in the summary section.

4.2.1 Case I

The first case is the control case for the entire study. The cell voltage is set around 690V as it is given in the VFD data sheet. In case I, the output of the VFD is directly connected to the motors loaded 100%, and there is no cable in between. Figure 48 shows the waveforms of this case. Table 6 shows the results of case I. VFD outputs and one of the motor outputs are same since there is no cable in between them.

Table 6: Case I Result

Case I		VFD Output			V_AB_Motor		
		THD (%)	MAX	RMS	THD (%)	MAX	RMS
	Voltage(V)	9.6	6946	4097	9.6	6946	4097
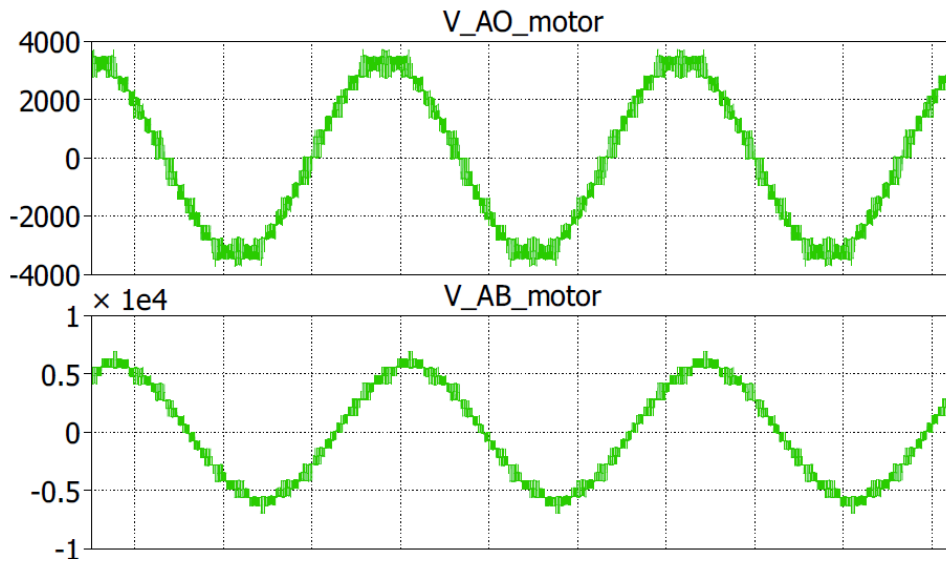
Figure 48: Case I-Full Load and no Cable Waveforms

4.2.2   Case II-A

In case II-A, the output of the VFD is connected to the motors loaded 100% through a 5-km long umbilical cable modeled as 10-Π section with the parameters given previously. The skin effect modeling of the cable is not included. Table 7 shows the result of Case II-A, and Figure 49 shows the waveforms.

Table 7: Case II-A Result

Case II-A		VFD Output			V_AB_Motor		
		THD (%)	MAX	RMS	THD (%)	MAX	RMS
	Voltage(V)	9.6	6952	4102	44	9107	4144
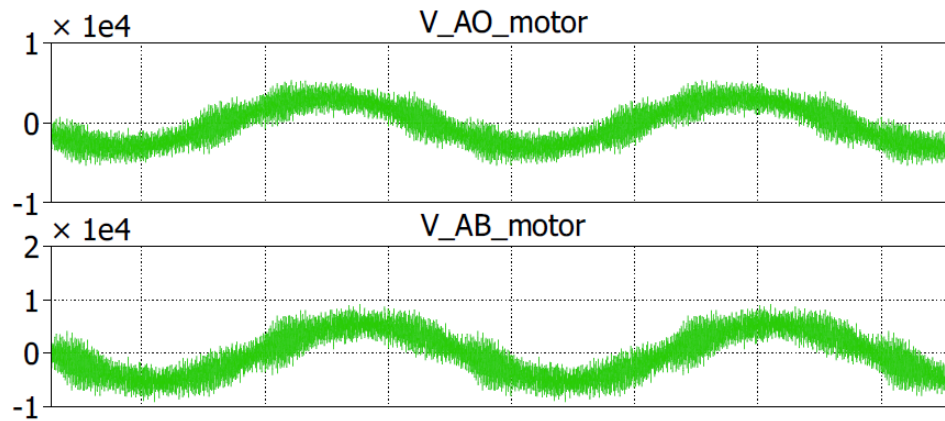
Figure 49: Case II-A-Full Load with 5km Cable

4.2.3 Case II-B

In case II-B, the output of the VFD is connected to the motors loaded 100% through a 20-km long umbilical cable modeled as 45-Π section with the parameters given previously. The skin effect modeling of the cable is not included. Table 8 and Figure 50 show the results and waveforms of this case study.

Table 8: Case II-B Result

Case II-A		VFD Output			V_AB_Motor		
		THD (%)	MAX	RMS	THD (%)	MAX	RMS
	Voltage(V)	9.6	6972	4113	45	8135	3413
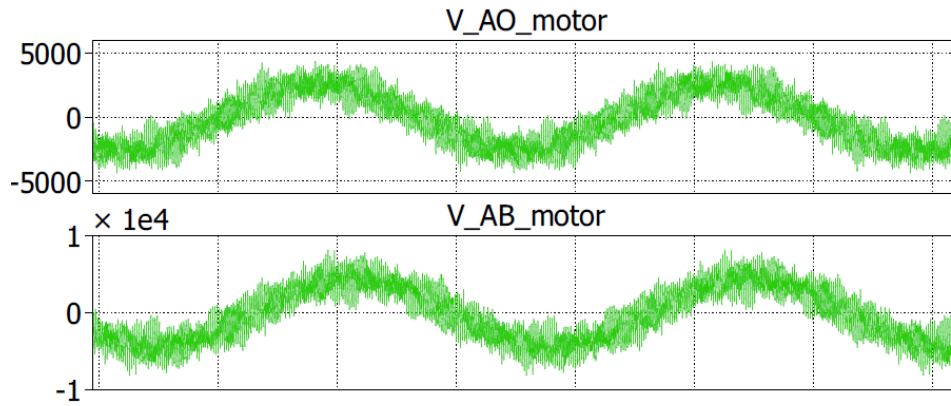
Figure 50: Case II-B-Full Load with 20km Cable

4.2.4 Case III-A

In case III-A, the output of the VFD is connected to the motors loaded 100% through a 5-km long umbilical cable modeled as 10-Π section with its skin effect modeled as explained previous chapters. Table 9 and Figure 51show the results and the waveforms of this case.

Table 9: Case III-A Result

Case III-A		VFD Output			V_AB_Motor		
		THD (%)	MAX	RMS	THD (%)	MAX	RMS
	Voltage(V)	9.6	6952	4102	13.5	7241	3816
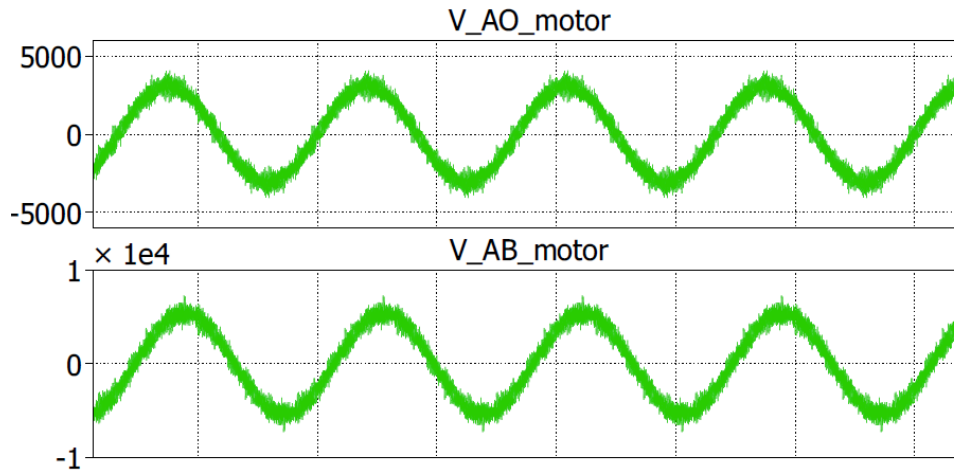
Figure 51: Case III-A-Full Load with 5km Cable Including Skin Effect

4.2.5 Case III-B

In case III-B, the output of the VFD is connected to the motors loaded 100% through a 20-km long umbilical cable modeled as 45-Π section using the parameters given previously. Skin effect is included by using the skin effect model explained in previous chapters. Table 10 and Figure 52 show the results and the waveforms of this case study.

Table 10: Case III-B Result

Case III-B		VFD Output			V_AB_Motor		
		THD (%)	MAX	RMS	THD (%)	MAX	RMS
	Voltage(V)	9.6	6972	4113	20.8	6708	3172
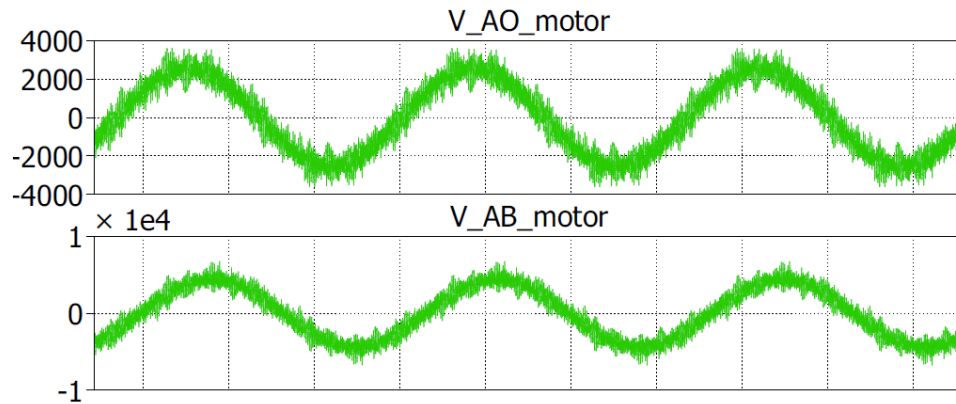
Figure 52: Case III-B-Full Load with 20km Including Skin Effect

4.2.6 Case IV-A

In case IV-A, the output of the VFD is connected to the motors loaded 100% through a 5-km long umbilical cable modeled as 10-Π section with its skin effect using the parameters given previously. A passive L filter with a value of 1.8mH is connected in series at the output of the VFD for this simulation. Table 11 and Figure 53 show the results and the waveforms of this case.

Table 11: Case IV-A Result

Case IV-A		VFD Output			V_AB_Motor		
		THD (%)	MAX	RMS	THD (%)	MAX	RMS
	Voltage(V)	9.6	6962	4108	11.8	5909	3688
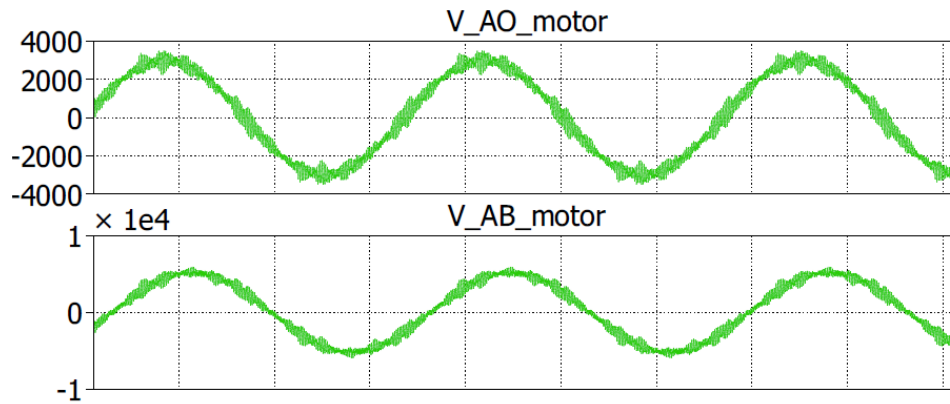
Figure 53: Case IV-A-Full Load with 5km Cable and a Filter

4.2.7 Case IV-B

In case IV-B, the output of the VFD is connected to the motors loaded 100% through a 20-km long umbilical cable modeled as 45-Π section with its skin effect using the parameters given previously. A passive L filter with a value of 1.8mH is connected in series at the output of the VFD for this simulation. Table 12 and Figure 54 show the results and the waveforms of this case.

Table 12: Case IV-B Result

Case IV-A		VFD Output			V_AB_Motor		
		THD (%)	MAX	RMS	THD (%)	MAX	RMS
	Voltage(V)	9.6	6982	4118	6	4511	3030
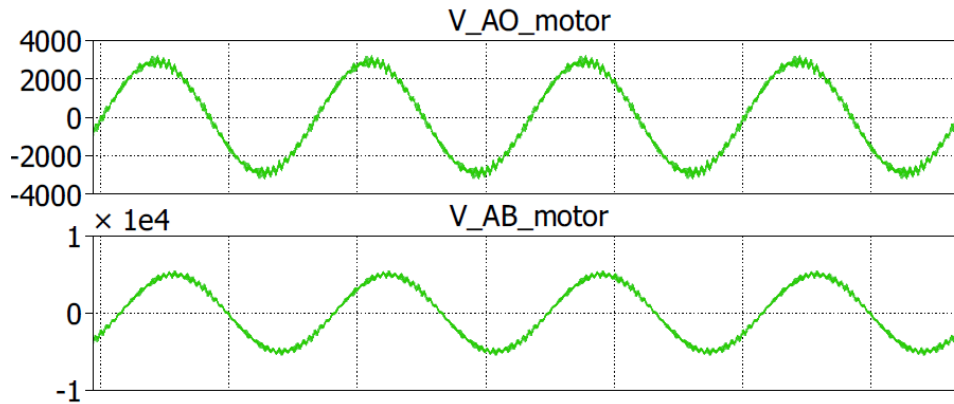
Figure 54: Case IV-B-Full Load with 20km Cable and a Filter

4.3 Summary

Table 13 shows the summary of all the results. High frequency effects of VFDs on ESP systems can be seen by comparing the results. If there was no umbilical cable in the system, the motor would be connected to the VFD output, thus motor terminal voltages would be known, and there would be no uncertainties. Depending on the PWM scheme and type of the VFD, there is certain dominant harmonics at the output of the VFDs. For multilevel inverters dominant harmonics will be around the switching frequency of the drive. For multi-level H-bridge inverters, the switching frequency of the VFD can be calculated as;

$$f_{VFD} = 2Hf_{switching}$$

$$f_{13-level-inverter} = 2 \times 6 \times 900 = 10800 Hz$$

Here, $f_{switching}$ is the switching frequency of the easch H-bridge power cell, thus, 36 pulse multilevel (13 levels) VFD has dominant harmonics around 10800Hz. This is shown in Figure 55.

Case I shows the output voltage of the 36 pulse multilevel VFD. Total harmonic distortion is 9.6% and maximum voltage level is about 6900V. There is no uncertainty in the system for the Case I. However, by introducing umbilical cable in the system, motor terminal voltage is hard to determine. When dominant harmonics of the VFD voltage output coincides with the resonant points of the cable, magnitudes of these harmonics are amplified. Thus, total harmonic distortion at the end of the umbilical cable is higher due to the amplification of the harmonics. Figure 55 explains how the amplification occurs for Case II-A. It occurs in a similar way for Case II-B as well. As a result of this amplification, in Case II-A and Case II-B, THD values of the motor terminal voltages jump around 44-45%, and voltage spikes are seen around 9 kV.

Table 13: Summary of the Results

100% Loaded CASE	VFD Output			V_AB_Motor			
	THD (%)	MAX	RMS	THD (%)	MAX	RMS	Fund.
Case I : No cable	9.6	6946	4097	**9.6**	**6946**	4097	**4078.6**
Case II-A : Cable(5km)	9.6	6952	4102	44	9107	4144	3783
Case II-B : Cable(20km)	9.6	6972	4113	45	8135	3413	3109.9
Case III-A : Cable(5km)& skin effect	9.6	6952	4102	13.5	7241	3816	3782
Case III-B : cable(20km)& skin effect	9.6	6972	4113	20.8	6708	3172	3105
Case IV-A : cable(5km)& skin effect &filter	9.6	6962	4108	11.8	5909	3688	3663
Case IV-B: Cable(20km)& skin effect &filter	9.6	6982	4118	6	4511	3030	3025
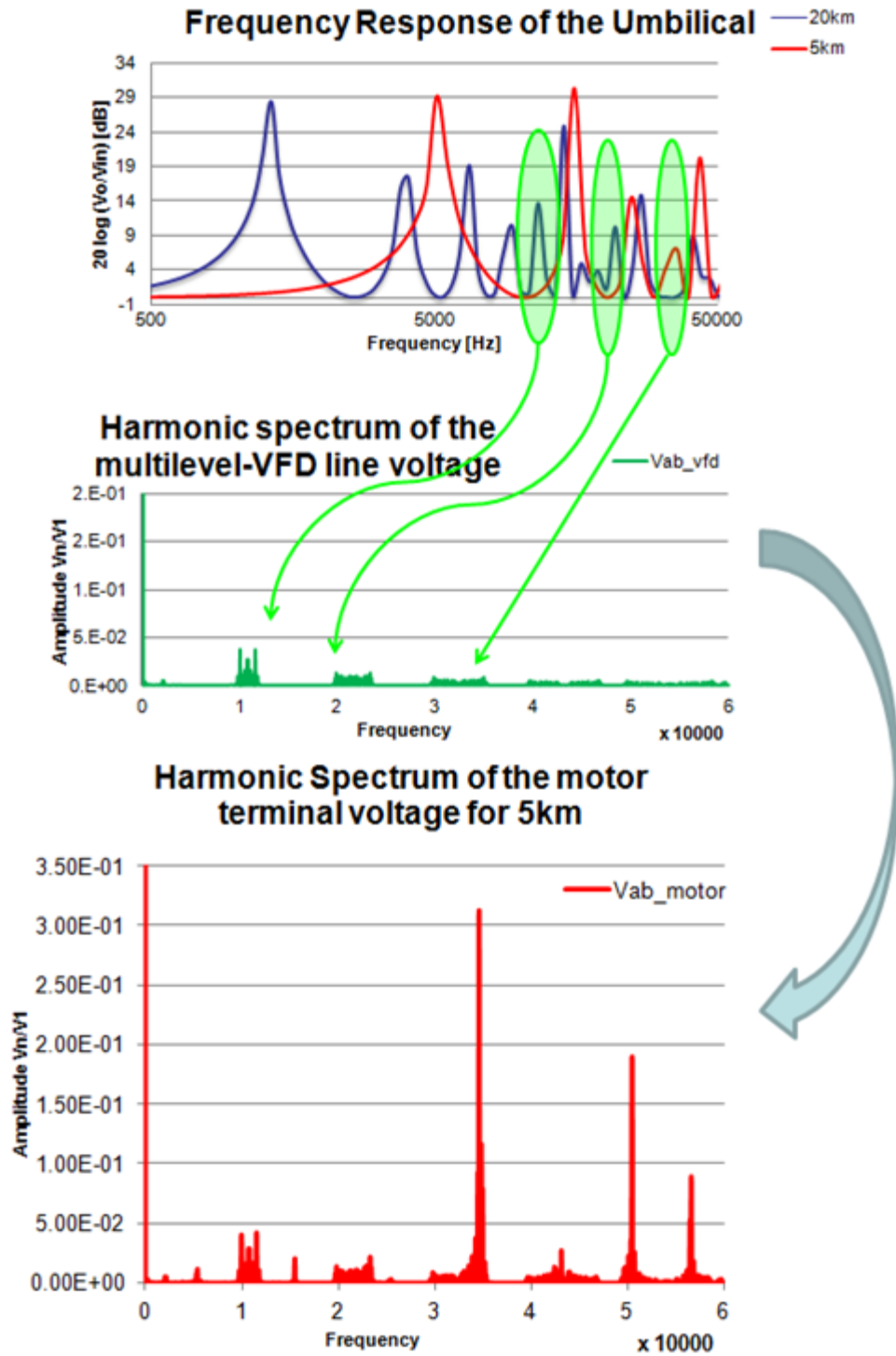
Figure 55: Amplification of Harmonics

Skin effect occurs at high frequencies on the cables. It reduces internal inductance of the cables and increases the resistance as it is explained previously. Due to this change in inductance of the cables, resonant points of the cable shifts slightly to higher frequencies. Due to the increase in resistance, the voltage gain on resonant points is damped. The frequency response difference between 50Hz parameters of the cables and frequency-dependent parameters was shown in Figure 24 and Figure 25 for 20-km and 5-km long cables respectively. Thus, amplification occurs with lower values of voltage gains for harmonics, and total harmonic distortion of the motor terminal voltage becomes lower than the cases without the skin effect model. It is clear that in Case III-A and Case III-B, due to the skin effect modeling, THD value of the motor terminal voltage reduces to 13.5% and 20.8%. These are due to the increase in resistance values. It needs to be pointed that fundamental values should not be affected from the skin effect modeling. Since skin effect model changes the parameters for higher frequencies, only higher frequencies should be affected from that. Thus, by comparing Case II-A with III-A and Case II-B with III-B, it can be seen that fundamental values are nearly not changed. Therefore, the skin effect model meets the expectations.

Case IV-A and Case IV-B explain the effect of harmonic filters on ESP systems. These resonance points of the cables can be easily attenuated by using filters. Figure 56 and Figure 57 shows the frequency responses of 5-km and 20-km system with and without the filter, respectively. For both examples, the same filter is used. It is obvious that, with a simple harmonic filter, resonant points can easily be attenuated and damped. Motor terminal voltage THD values and maximum terminal voltages are lowered.
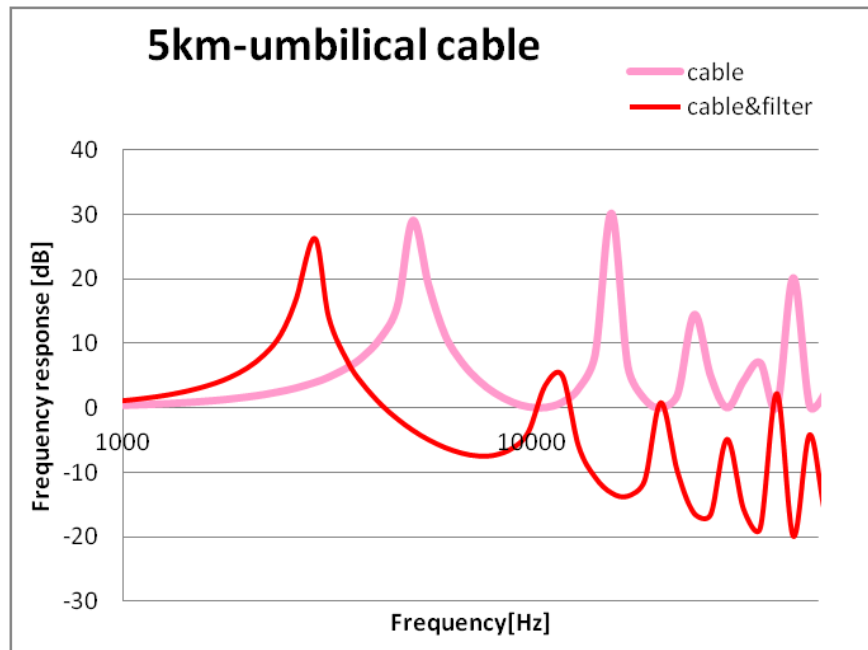
Figure 56: Frequency Response of 5km Cable with and without the Filter
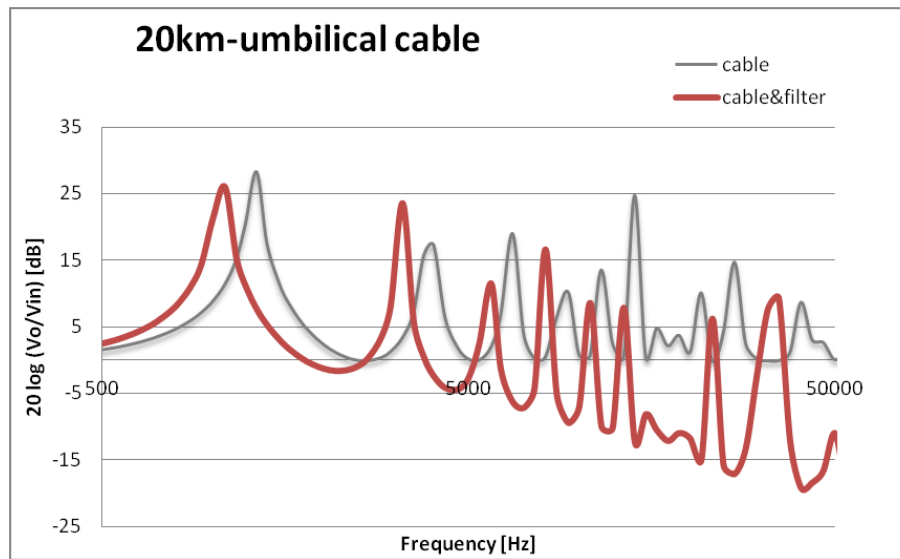
Figure 57: Frequency Response of 20km Cable with and without the Filter

5. CONCLUSIONS & FUTURE WORK

High frequency effects of VFDs on ESP systems are studied. It is shown that, the result of the system is heavily dependent on;

- Cable length

- Cable parameters

- VFD-type

- PWM scheme

- Frequency modulation index(mf)

- Amplitude modulation index(ma)

- Frequency Dependent Modeling of cable

- Filter

In order to analyze these systems, first physical conditions of the system should be determined. After the length between the power source and the ESP motors are defined, harmonic study for different combinations of VFDs and umbilical cables should be performed. Since harmonic spectrum of each VFD and frequency response of each cable is different, best combination for the specified length should be selected. Harmonic filter should be designed to avoid possible voltage spikes on motor terminal voltages due to the resonances on the cable.

In this project, the configuration shown in Figure 42 is studied for 5km and 20km lengths. In this system, two ESP systems are connected to VFDs through an umbilical cable. High frequency modeling of the cable and 36 pulse-multilevel VFD modeling is performed for the harmonic studies. Resonance issues is addressed and shown with figures and results. Results show the importance of harmonic studies for ESP systems.

Besides harmonic studies, another important point related to this configuration is voltage drop issues. The fundamental values of the voltage in Case II-A and Case II-B shows that as the length increases, voltage drop increases as well. Voltage drop reached up to 25% for 20km long cable in this configuration. This issue may lead to motor starting issues; therefore, motor starting analysis should be performed in these systems. There are more factors related to motor starting, therefore, this is left as a future work.

As it is mentioned earlier, in case of using all the three phase cables in the cable shown in Figure 44, there might be imbalances in voltages due to induced voltages, resulting in torque pulsations. This study is also left as a future work.

REFERENCES

[1] X. Liang, S. O. Faried, and O. Ilachonwu, "Subsea cable applications in electrical submersible pump systems," IEEE Trans. Ind. Appl., vol. 46, no. 2, pp. 575-583, March/April 2010.

[2] B. Wu, *High-Power Converters and AC Drives*, NJ: John Wiley&Sons, 2006.

[3] *IEEE Recommended Practices and Requirements for Harmonic Control in Electrical Power Systems*, IEEE Std.519-1992, NY, 1992.

[4] J. Smith, "Selection of transmission circuit models for power-system transient studies," in *IEE Proc.C Generation Transmission & Distribution,* vol.131, Pt.C, no.1, pp. 1-4, Jan 1984.

[5] C. R. Paul, *Loop and Partial*, John Wiley & Sons, Inc., 2010.

[6] J. Oliveira, "Electrical transmission system with variable frequency through long length cable," *Houston Offshore Technology Conference*,TX, 6-9 May 1996, pp. 271-280.

[7] R. L. Wheeler, and Bidyut K.Sen, "Skin effects models for transmission line structures using generic SPICE Circuit Simulators," in *Proc. IEEE Meeting Electrical Performance Electronic Packaging*, Oct. 1998, pp. 128-131.

[8] Chu-Sun Yen, Z. Fazarinc, R. L. Wheeler, "Time domain skin effect model for transient analysis of lossy transmission lines," in Proc. of *IEEE,* Vol.70, No. 7,pp 750-757, July 1982.

[9] Joable Andrade Alves, Gilberto da Cunha, and Paulo Torri, "Medium Voltage Industrial Variable Speed Drives," WEG Application Note, the last day retrieved May 2012, http://catalogo.weg.com.br/files/wegnet/WEG-medium-voltage-industrial-variable-speed-drives-technical-article-english.pdf

[10] M. H. Rashid, *Power Electronics Circuits,Devices, and Applications*, NJ: Prentice-Hall, 1993.

[11] N. Mohan, *Power Electronics Converters,Applications and Design*, John Wiley& Sons Inc., 2003.

[12] E. Cengelci, "Multilevel inverters and modular adjustable speed drive systems," Dissertation, Texas A&M University, College Station, TX, August 2000.

[13] Peter W. Hammond, "Medium voltage PWM drive and method," United States Patent 005,625,545, Appl. No: 203,803, Halman Rabicon Group, PA, pp. 1-21, 1 March 1994.

APPENDIX A

General Cable
ex ZH ellent XXI
EL CABLE DEL NUEVO SIGLO

Offer nº :
Order nº :
Page nº : 1

	MEDIUM & HIGH VOLTAGE CABLES	Units	ITEM1
1	Cable code		0341835
2	Cable type		RHE-2OL
3	Standard		IEC 60502-2
4	Nominal voltage	kV	12/20
5	Nº of cores x C.S.A.		1 x150 mm²
6	Conductor material		Cu
7	Shape		Circular
8	Class / Standard		2 / CEI-60228
9	Nominal diameter	mm	14,95
10	W.B. conductor		YES
11	Swellable semi-conducting tape over conductor		NO
12	Conductor screen material		Extruded semi-conducting layer
13	Nominal radial thickness	mm	1,2
14	Insulation material		XLPE
15	Nominal radial thickness	mm	5,5
16	Nominal diameter over insulation	mm	29,2
17	Insulation screen material (non metallic)		Extruded semi-conducting layer
18	Nominal radial thickness	mm	0,6
19	Swellable semi-conducting tape under metallic screen		NO
20	Insulation screen (metallic)		CWS
21	Nº of wires x Diameter	N x mm	60x0,584
22	Nominal tape thickness / Overlap	mm / %	
23	C.S.A. (Cu wires)	mm²	16
24	W.B. metallic screen (swellable yarn)		YES
25	Swellable tape over metallic screen		NO
26	Metallic / Copolymer tape		NO
27	Nominal total C.S.A. (Cu wires + Metal/Copolymer tape)	mm²	16
28	Metallic sheath bedding material		N/A
29	Nominal radial thickness	mm	
30	Metallic sheath material		N/A
31	Nominal radial thickness	mm	
32	Armour bedding material		N/A
33	Nominal radial thickness / Minimum at any point	mm	
34	Armour material		N/A
35	Nominal under armour diameter	mm	
36	Nº of wires (approx.) x Diameter / Metallic uncounter tape	N x mm	
37	Nominal tapes thickness	mm	
38	Outer sheath material		HDPE
39	Nominal radial thickness / Minimum at any point	mm	2,0 / –
40	Nominal overall diameter	mm	36,0
41	Minimum overall diameter	mm	35.9
42	Maximum overall diameter	mm	37.4
43	Nominal total weight	kg/km	2325
44	Minimum bending radius	mm	509
45	Maximum conductor DC resistance, at 20 ºC	Ohm/km	0,124
46	Star reactance per phase, at 50 Hz	Ohm/km	0,115
47	Capacitance per phase	µF/km	0,252
48	Charging current per phase, at Uo, 50 Hz	A/km	0,949
49	Maximum permanent current rating (*)	A	435 (1) / 340 (2)
50	Maximum conductor temperature in service / in short-circuit	ºC	90 / 250
51	Maximum adiabatic short-circuit current rating (0.1/0.5/1.0 s)	kA	67,8 / 30,3 / 21,4

(*) In air, at 40 ºC / Buried, at 25 ºC - 1,6 ºK·m/W - 1 m (see more details in ANNEX)
NIA = Not Applicable
Nominal values subject to the usual manufacturer tolerances

Signed by : F. Galante
Date : 05/06/2008

General Cable reserves the right to change or modify the specifications and materials depending on future improvements. Based on this, data listed above could be modified due to these changes

Figure 58: Umbilical cable datasheet

APPENDIX B

Variable Speed Drive Data Sheet Gen IIIe A5E03334316A REV AC		
Description	**Unit**	**Specification**
Project		PAI-Cascade & Chinook
Purchase Order		47115054/EWHG
Sales Order		3001366105
Drawing/VFD Part Number (4)		A5E02060-534/535/536/537
Model		Siemens LDA Perfect Harmony, Gen IIIe - NXG Control
Dimensions (HxWxD)	inches	120.21 x 326.00 x 54.00
Weight	lbs	36,900.00
Technology		Voltage Source
Microprocessor-based Multilevel Switching		Multi-Level PWM
Supply Voltage	V	11,000
Tolerance	%	+10%, -5%
Supply Frequency	Hz	60
Number of Phases		3
Frequency Tolerance (Steady State)	%	+5, -5
Frequency Tolerance (Transient Duration 1.5s)	%	+10, -10
Transformer KVA Rating	kVA	3000
Rectifier Device		Diode
Inverter Device		IGBT
Cell Voltage	V	690
Cell Current Rating	A	315
Number of Cells		18
Number of Pulses		36
Blower Voltage	V	460
Control and Heater Power	V	240
Low Voltage Control	V	120 VAC by Siemens Large Drives Siemens LDA
DC Link Capacitor		Yes
Input Power Factor(30% - 100% speed)	Cos f	95
Voltage Cut Ride Through Duration		5 Cycles
Volt Dip (w/ cont operation)	%	30%
VFD Output Voltage (max)	V	7200
VFD Output Current (max)	A	315
Output Frequency	Hz	0-60
Speed Control	Hz	.1 Hz
Overload Capability	%	110% for 60s every 10m
Torque Pulsations Across Speed Range	%	Maximum of .01 of 1%
Quadrant Of Operation w/ Vector Control		2
Cooling		Air
Enclosure Protection Rating		IP42
Ambient Temperature Max	Deg C	40
Humidity (non-condensing)	%	95
Altitude	ft	3300
Manuals Provided In Language		English
VFD Output Voltage (max) at -8.5% Supply Voltage	V	6700
XFMR kVA Rating at 45deg C	kVA	2850
Cell Current Rating at 45deg C	A	259

Figure 59: VFD datasheet

APPENDIX C

Motor Data Sheet

BAKER HUGHES

		Date:	30-Nov-09
		Prepared by:	GDI

Project Information				
Customer Name	FMC Technologies	Project Name	Cascade and Chinook	
Region	Gulf of Mexico	Project Number	1231	
		Document Number	1231-06-006	
Field Name	Cascade & Chinook	Revision	A	
Well Name		Part Number	C308864	

ITEM	DESCRIPTION	VALUES	Document Reference
1	General Parameters-		
1.1	Motor Construction, Size and Characteristics	HMI - X VANGUARD CONSTRUCTION 850HP 4239 V 120A	
1.2	Motor Series	725 Series	
1.3	Diameter	7.25" O.D.	
1.4	Length	36.5 ft	
1.5	Weight	4,630 LB	
1.6	Number of Rotors	16	
2	Performance Ratings		
2.1	BHT	Varies	See DOC# 1231-12-004
2.2	Motor Temperature Rating (F)	425F - Max	
2.3	Rotor Loading (HP / Rotor)	53.12	
2.4	Horsepower per Rotor	53.12	
2.5	Rated HP & Frequency (nameplate)	850HP 60Hz	
2.6	Motor Terminal Voltage – Nominal	4239 V nom	
2.7	Motor Terminal Voltage – Minimum	3985 V min	
2.8	Motor Terminal Voltage – Maximum	4493 V max	
2.9	Min Motor Terminal Starting Voltage	1696	
2.10	Full Load Amps	120A	
2.11	Full Load Efficiency	87	
2.12	Full Load Power Factor	0.85	
2.13	Full Load Slip	106 rpm	
2.14	Full Load Torque	1277	
2.15	Motor Inertia (lb-ft^2)	12.51	
3	Basic Type Materials		
3.1	Housing	13 Cr	
3.2	Head and Base	410 SS	
3.3	Shaft	4130 Alloy Steel	
3.4	O-rings	CL-180	
3.5	Fasteners	Nickel K500	
3.6	Pothead	Monel	
3.7	Exterior Coating	Centrilift Standard Paint	
4	Design Features-		
4.1	Configurations (Single, LT, UT)	Single	
4.2	Construction Type(Vanguard,etc)	Vanguard	
4.3	Oil Type	CL-5E	
4.4	Sensor (yes/no)	Yes	
4.5	Sensor type	Sureflo Pod for Harvest Electronics	
4.6	MWT sensor type (RTD, etc)	RTD	
4.7	Connection Class	WYE	

REMARKS (special requirements)

Figure 60: ESP motor data sheet

VITA

Esra Ozkentli received her Bachelor of Science degree in electrical engineering in 2008 from Istanbul Technical University, Istanbul, Turkey. She worked in the Advanced Electric Machines and Power Electronics Laboratory in the Department of Electrical Engineering at Texas A&M University under the supervision of Dr. Hamid Toliyat, and obtained her Master of Science in electrical engineering in August 2012.

She may be reached at esraozkentli@gmail.com or through the Department of Electrical and Computer Engineering, Texas A&M University, 3128 TAMU, College Station, Texas 77843.